Journal of Materials Chemistry B

ROYAL SOCIETY OF CHEMISTRY

REVIEW

View Article Online
View Journal | View Issue

Cite this: J. Mater. Chem. B, 2022, 10, 2296

Recent progress in tannic acid-driven antibacterial/antifouling surface coating strategies

Gnanasekar Sathishkumar,[a] Kasi Gopinath,[a] Kai Zhang,[a] En-Tang Kang,[ab] Liqun Xu *[ac] and Yunlong Yu *[de]

Received 22nd September 2021,
Accepted 31st December 2021

DOI: 10.1039/d1tb02073k

rsc.li/materials-b

Medical devices and surgical implants are necessary for tissue engineering and regenerative medicines. However, the biofouling and microbial colonization on the implant surface continues to be a major concern, which is difficult to eradicate and typically necessitates either antibiotic therapy or implant removal. As a result, efficient and eco-friendly bioinspired coating strategies for tethering functional materials or molecules on different medical substrates are highly desirable, especially for endowing versatile surface functionalities. Tannic acid (TA), a well-known tea stain polyphenol, has a good affinity for various substrates and actively inhibits the adhesion and colonization of microbes. Thus, functionalization of polymers, nanomaterials, metal-phenolic networks (MPNs), and proteins using TA bestows the end-products with unique binding or anchoring abilities on various implantable surfaces. This review addresses the recent advancements in the essential biomedical perspective of TA-based bioinspired universal surface coating technologies by focusing on their intrinsic features and ability to produce engineered functional composites. Further, the possible contributions of TA-based composites in antifouling and antibacterial applications on various biomedical substrates are outlined.

1. Introduction

Implant-associated infections (IAI) are severe complications after implantation surgery and pose a significant risk to human health worldwide.[1,2] In particular, the colonization of planktonic bacteria on implant surfaces leads to three-dimensional biofilm formation, which remains a major issue in the healthcare sector.[3] Also, the adhesion of different micro/macro fouling agents has various implications, including malfunctions of medical devices and implants.[4,5] In the United States, catheter-associated biofilm formation has caused more than 200 000 intravascular and bloodstream infections each year.[6] The most frequent treatment approach for treating IAI is to replace old implants with new ones or to provide systemic antibiotics after surgery. However, there is a risk of recurrent infection in surgical replacement, leading to the lengthening of healing time and increasing patient morbidity.[7,8] Also, the systematic administration of antibiotics fights against bacterial infections, but their indiscriminate misuse resulted in the occurrence and prevalence of multidrug-resistant (MDR) superbugs.[9] To overcome these issues, few significant efforts were made to fabricate different molecular design-based surface coating strategies with antibacterial and antifouling properties.

Recently, many coating technologies have been established using bioactive ingredients such as biomolecules,[10] nanomaterials,[11] polymers,[12] minerals,[13] and antibiotics.[14,15] Usually, the coating has been developed by multiple techniques, including electrophoretic deposition,[16–20] magnetron sputtering,[21–25] thermal spray,[26] plasma-enhanced chemical vapour deposition,[27–29] pulsed laser deposition,[30] ion-beam processing,[31] physical grafting,[32] and chemically conjugated coatings.[33,34] The limitations of existing methods such as high energy consumption, form dependency, repeatability on many substrates, and time consumption must be addressed for a scaled-up approach.[35] Therefore, a simple mussel-bioinspired universal coating technique can be developed as a potential alternate for the site-specific and prolonged elimination of bacterial infections.[36] A growing interest has been given to natural products such as polysaccharides,[37] biomolecules,[38] and polyphenols-driven surface modifications[39] with unique properties. In particular, polyphenols have gained significant attention owing to their inherent broad spectrum of bioactivities. Apart from medicinal values, the active functional groups such as

[a] Chongqing Key Laboratory for Advanced Materials and Technologies of Clean Energies, School of Materials and Energy, Southwest University, Chongqing, 400715, China. E-mail: xulq@swu.edu.cn, yuyunlong666@gmail.com
[b] Department of Chemical and Biomolecular Engineering, National University of Singapore, Kent Ridge, 117576, Singapore
[c] Key Laboratory of Laser Technology and Optoelectronic Functional Materials of Hainan Province, College of Chemistry and Chemical Engineering, Hainan Normal University, Haikou, 571158, P. R. China
[d] National Engineering Research Center for Biomaterials, Sichuan University, 29 Wangjiang Road, Chengdu 610064, China
[e] Institute of Burn Research, Southwest Hospital, Third Military Medical University (Army Medical University), Chongqing, 400038, China

dihydroxyphenyl and trihydroxyphenyl of the polyphenols endow the engineering of advanced multifunctional materials.[40,41]

Tannic acid (TA) is a water-soluble natural polyphenol compound commonly found in grapes, tea extract, red wine and commercially produced using different plant entities.[42] As per the US Food and Drug Administration, TA is proven to be safe and non-toxic at minimal concentrations.[43] The general structure of TA ($C_{76}H_{52}O_{46}$) has a central glucose molecule with two esterified gallic acid (3,4,5-trihydroxybenzoic acid) on its five hydroxyl moieties.[44] Owing to the pyrogallol and catechol groups, TA possesses remarkable antibacterial,[45] antiviral,[46] and antioxidant[47,48] properties, rendering its overall biomedical perspective. TA's excessive phenolic functional groups provide good coordination sites for bioinspired surface engineering and post-modification applications.[49] Also, these reductive phenolic hydroxyls and multiple active sites of TA could serve as a natural reducing/exfoliating agent to fabricate various functional nanomaterials.[50–52]

In the past decade (*i.e.*, since 2013), the inherent affinity of TA and its metal ion (TA/Fe^{3+}) complex has been utilized as building blocks to construct ultrathin interface coatings on various substrates. The multiple active sites of TA provide strong interactions with different implant surfaces, protecting them from enzymatic degradation and reactive oxygen species (ROS) attack in the biological milieu.[44,49] Various physical and chemical interactions, including hydrogen bonds, hydrophobic interactions, electrostatic interactions, Michael addition/Schiff base reactions, and polyphenol–metal coordination compounds, contribute to TA-driven surface coatings.[53] As a result, diverse TA-driven surface engineering approaches have been practiced in contemporary materials science research *via* exploiting anti-adhesive films,[54,55] antimicrobial agents,[56] photoactive materials,[57–59] and cationic coatings.[60,61] Furthermore, these modified surfaces combat infectious bacterial colonization *via* releasing antibacterial agents, photothermal/photodynamic therapy, and contact-killing.

This review emphasis the present state-of-the-art information on interactions between TA-modified surface and active ingredients. We have also explicitly discussed the recent advancements and breakthroughs in developing TA-assisted universal bio-inspired surface coating technologies to deposit antibiotics, biomolecules, minerals, polymers, and nanomaterials. Only anti-biofilm and antifouling active coating formulations/compositions with significant biomedical applications (excluding energy and environmental prospects) were assessed and discussed relative to the scope of this review. With specific references to tissue engineering and regenerative medicine standpoint, all the provided information will bestow diverse techniques to fabricate TA-engineered multifaceted biomaterials and medical devices.

2. Tannic acid (TA)-based coatings

2.1. Layer-by-layer (LbL) deposition

LbL deposition is a facile and versatile method to prepare multifaceted coatings with unique structural and physiochemical features for the sustained release of active payloads. By modulating the assembly conditions, the LbL technique maintains uniformity in the film's content, morphology, thickness, and mechanical behaviour.[62,63] Using this strategy, different natural or synthetic polymers, nanomaterials, proteins, and polysaccharides were covalently and non-covalently integrated.[64,65] The LbL modified surfaces eliminate planktonic bacterial pathogens *via* contact-killing or releasing various active constituents like antibiotics, biomolecules, and metal ions.[66,67] With different coating techniques such as dip, spin, and spray coatings, the LbL assemblies have been used to construct either adhesion resistant or release killing surfaces. Among them, dip and spin coating techniques were largely explored in biomedical implant surface coating modification.[68–70]

According to reported studies, the pK_a range of TA varies between 2.5 to 8.5 based on the different tannin sources.[71,72] TA can operate as a weak acid due to its strong ionization rate of polyphenol groups at pH 7.5. These dynamic functional characteristics of TA led to its use as a building block in the LbL method. Ultimately, the TA could react with neutral or positively charged materials or molecules *via* a series of interactions, including hydrogen and covalent bondings, hydrophobic, electrostatic, π–π interactions, as well as metal–polyphenol coordination complexes (Fig. 1).[40,43,73] For instance, the formation of hydrogen bonds between different neutral polymers with TA results in multilayer anionic polymer/TA film generation at a pH of 7.5. The switchable pH dissolution behavior of polymer/TA film can deliver various active materials or molecules in a controlled manner.[74] Zhuk *et al.* reported an effective LbL deposition for the direct assembly of TA with antibiotics like tobramycin, gentamicin (G), and polymyxin B. At physiological pH (7.5), the positively charged antibiotics can electrostatically bind with partially ionized TA. The LbL deposition of TA/antibiotic films was achieved through dip- and spin-assisted coating technology. Compared with the dip process, the spin-assisted technique generated surface with controlled morphology, roughness, and thickness.[75] Likewise, a dip-coating method was adopted to construct TA/G multiple bilayers coated nanoporous titanium (Ti) surfaces with different topologies (*i.e.*, smooth, 2D-nanoporous, and 3D-nanopillared). The pore size and thickness variation denoted the surface modification after the LbL deposition of TA/G film (9-layers) on three Ti surfaces. The apparent water contact angle (WCA) of TA/G-coated smooth, 2D-nanoporous, and 3D-nanopillar TiO_2 surfaces were 50°, 35°, and 0°, respectively, suggesting that the TA/G-coated surfaces were hydrophilic in nature. Also, it was noted that the TA/G coating bestowed on-demand delivery of drugs in orthopedic implants.[76]

It was a well-established fact that TA's trihydroxyphenyl moieties involve metal chelation to form tridentate complexes on stainless steel (SS) substrates, which can be alternatively deposited with biomolecules (parasin I peptide) in the LbL method (Fig. 2).[77] Recently, it was reported that utilization of two different buffers (acetate or citrate buffers) in TA and collagen type I (COL) based LbL film has shown a substantial impact on their morphology and antibacterial efficiency. The thickness variation and water absorption were recorded from

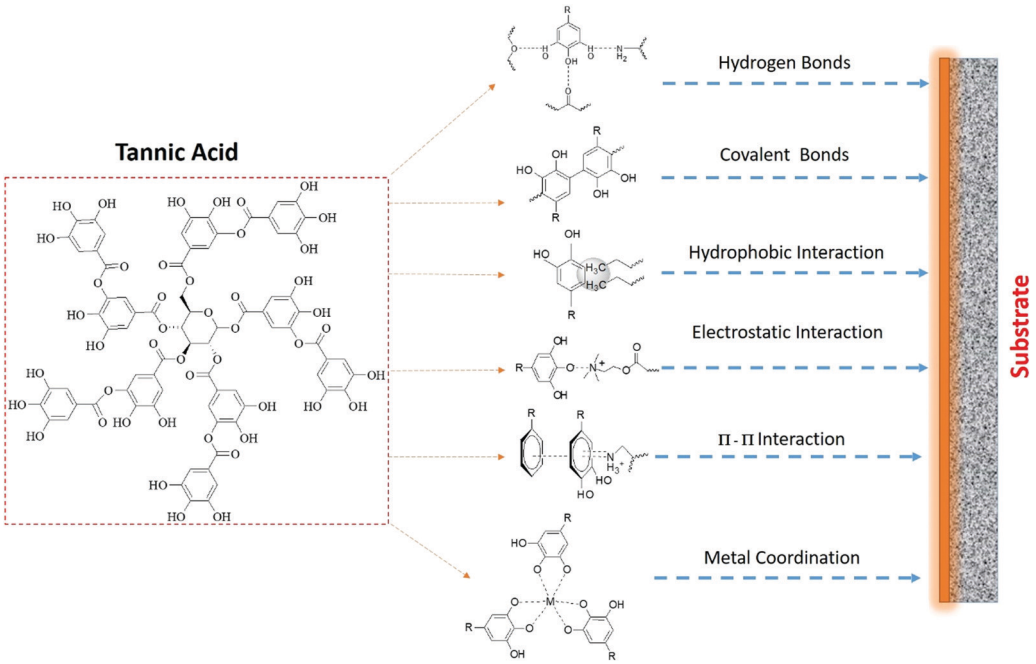

Fig. 1 Schematic of the various interactions contributing to TA-based bioinspired surface coatings.

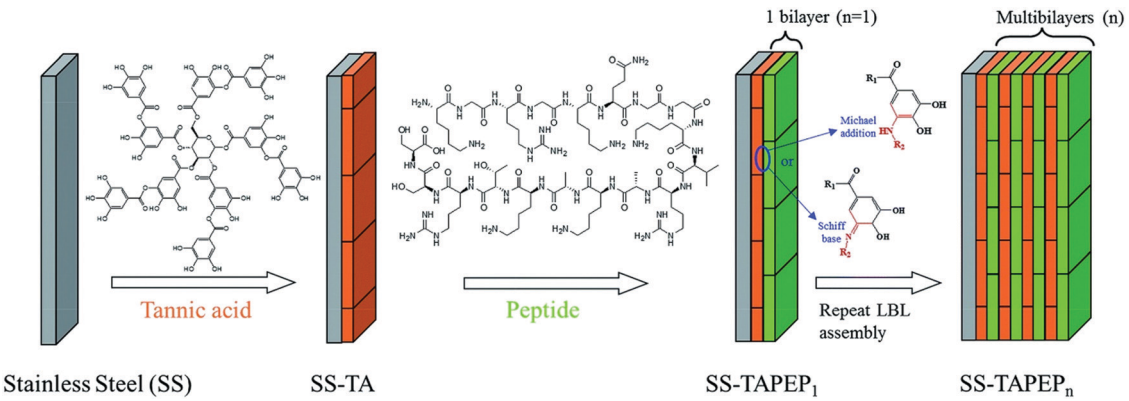

Fig. 2 Schematic of the preparation of multilayer coatings *via* LbL deposition on the SS surface (reprinted with permission from ref. 77. Copyright © 2016, Royal Society of Chemistry).

the Quartz Crystal Microbalance with Dissipation (QCM-D) measurements using the Voigt–Voinova model. Further, the microscopic images showed more fibrillary structures in acetate films, whereas granular ones were observed for citrate films. The results of Isothermal Titration Calorimetry (ITC) proved that the interaction of TA/COL was mediated by strong (citrate) and weak (acetate) hydrogen bond formation.[78] The LbL based deposition of TA-functional building blocks combined with antibacterial agents has been applied mainly in osteogenic implants, stimulating enhanced cellular attachment and proliferation.

2.2. Electro- and UV-assisted deposition

Fabrication of bioactive/nanomaterials coatings on various implant surfaces was achieved *via* multiple physical and chemical techniques. The UV-assisted and electrodeposition (ECD) methods have recently received much attention due to their cost-effectiveness, low energy consumption, and rapid deposition rate on complex-shaped substrates.[79–81] ECD is a feasible approach to produce polymers and nanomaterials coating in combination with TA. Electrode reactions, depletion forces, electrolyte flocculation, electrohydrodynamic fluxes, inorganic particle coagulation, and polymers contribute to the ECD process through various mechanisms and interactions. In the case of neutral polyvinylpyrrolidone (PVP) deposition, the active form of PVP–TA complexes *via* hydrogen bonding was considered as a crucial step. Owing to the partial deprotonation of the phenolic hydroxyl groups of TA, the solution became negatively charged, and the decreased local pH at anode triggered the protonation of TA and charge neutralization of the PVP–TA complexes. Moreover, it was suggested that the

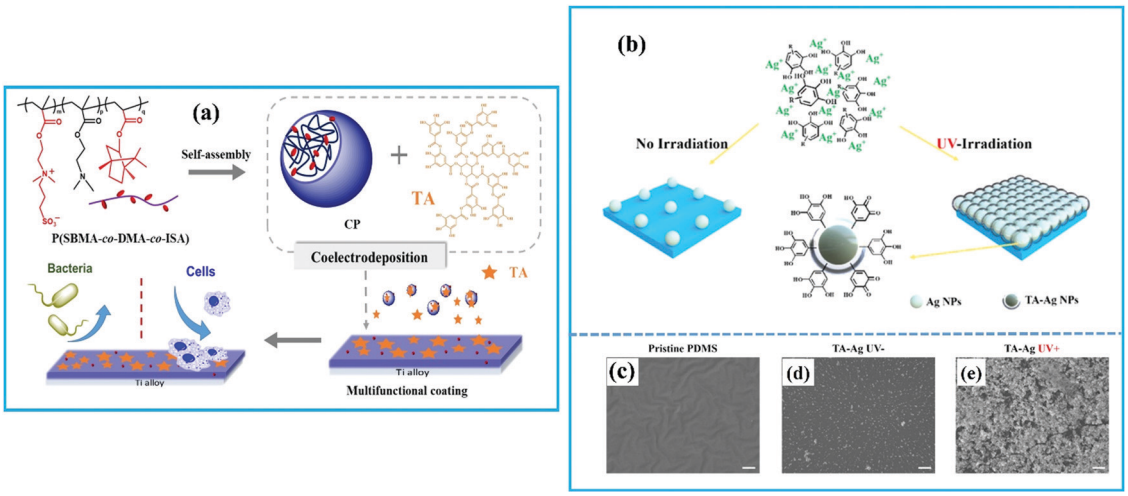

Fig. 3 (a) Schematic of the zwitterionic composite coating prepared by the ECD of polymeric colloidal particles and TA (reprinted with permission from ref. 84. Copyright © 2018, American Chemical Society). (b) Schematic of UV-assisted reduction and deposition of TA-Ag NPs on the surface. (c–e) SEM micrographs of the pristine polydimethylsiloxane (PDMS), PDMS-TA-Ag (UV^-), and PDMS-TA-Ag (UV^+) surface (reprinted with permission from ref. 85. Copyright © 2021, American Chemical Society).

accumulation of PVP–TA complexes at the electrode surface and the protonation of the phenolic hydroxyl groups of TA resulted in the TA bonding to different PVP molecules. The TA molecules, containing multiple galloyl groups, acted as cross-linkers and promoted insoluble PVP–TA films formation.[82]

Colloidal nanoparticles of TA self-suspended poly(isobornyl acrylate-*co*-dimethylaminoethyl methacrylate) were deposited on an Mg alloy substrate using the ECD method. Consequently, a smooth, thick, non-porous, and consistent polymer coating could be formed onto Mg substrates with strong adhesion, resolving some of the concerns with Mg-based implants.[83] Meng and co-workers demonstrated that the positively charged zwitterion polymer and TA mixture migrated toward Ti alloy (cathode) surface under an applied electric field, encouraging the formation of a concentration gradient of coating mixture around the Ti alloy surface. In addition, the increased pH near Ti alloy due to the electrolytic effect caused a reduction in the surface charge of polymeric colloidal particles, which resulted in flocculation of electrolyte and deposition on the surface (Fig. 3a).[84] It is noteworthy that the TA not only promoted affinity between active payload and substrate but also used to form anodic films in the ECD method.

Conversely, the UV-assisted techniques enable fast deposition of different inorganic nanomaterials onto implant surfaces in liquid-phase media.[86,87] As a breakthrough, UV-irradiation has recently been discovered to enhance the redox reaction between TA and Ag^+, resulting in accelerated nucleation growth and deposition of AgNPs (Fig. 2b). Compared to pristine PDMS (Fig. 2c) and without UV (Fig. 2d), the UV-irradiated PDMS showed the rapid deposition of monodispersed AgNPs (Fig. 2e), demonstrating the importance of UV-irradiation in attaining superior antibacterial surfaces.[85] Upon the UV-irradiation, the rate of oxidative polymerization of polyphenol increased rapidly and resulted in substrate-independent regulated deposition with unique coating patterns.[88]

3. TA-Tethered functional materials

3.1. TA-Tethered polymeric systems

Due to their versatility and biocompatibility, polymer-based surface coatings have got a lot of attention for their potential to resist IAI and biofouling.[89,90] Various functional polymers, including hydrophilic,[91] cationic,[92,93] and zwitterion[94] coating materials, have been extensively studied to modify different biomedical substrates. In particular, the cationic and zwitterion polymers are well-recognized candidature for developing anti-fouling/antibacterial coatings due to their excellent water molecule affinity and bacterial cell membrane disrupting properties. The existing mussel foot proteins (MFPs)-inspired adhesive agents, including polydopamine, catechol, and 3,4-dihydroxyphenylalanine (DOPA), have been successfully used to deposit functional polymers.[95] However, there is a growing demand for bioinspired compounds in universal coating applications over a wide range of substrates. For example, TA was considered as an ideal and sustainable alternative surface anchoring agent to fabricate polymer-based multifunctional coatings.

Polymer brushes deposited using the "grafting-from" approach had a better grafting density over the brushes tethered *via* "grafting-to" technique. Also, the bioinspired TA integration presents a sustainable surface modification strategy *via* surface-initiated graft-polymerization. Pranantyo *et al.*[96] used brominated TA (TABr) as an initiator primer for anchoring polymer brushes onto various substrates. Initially, the introduction of α-bromoisobutyryl bromide (BiBB) with TA generated TABr *via* nucleophilic *O*-acylation and TA-trihydroxyphenyl moieties partial esterification (Fig. 4a). The trihydroxyphenyl containing-TABr possessed affinity towards various metal and polymer substrates *via* tridentate metal complexes, hydrogen bonding, and hydrophobic interactions. After the surface grafting of polymer brushes *via* atom transfer radical polymerization (ATRP) of [2-(methacryloyloxy)ethyl]trimethylammonium chloride

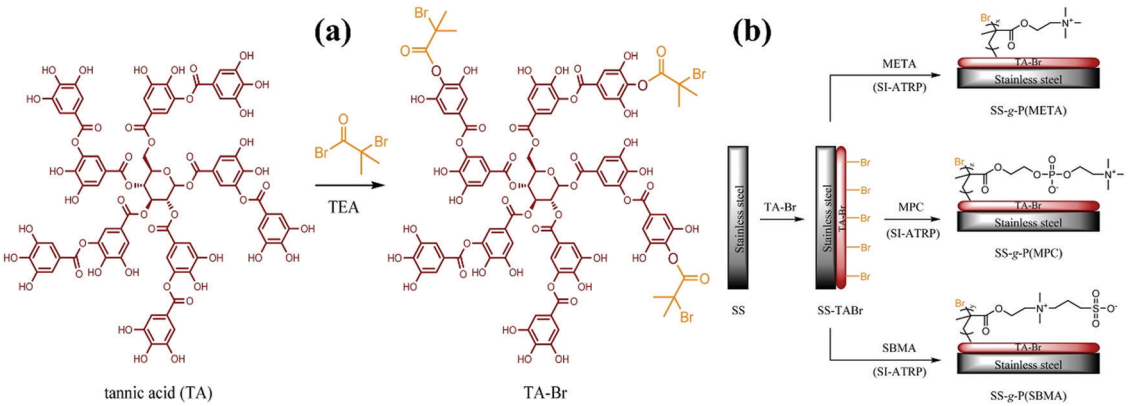

Fig. 4 (a) Synthesis of the TABr initiator primer through bromination of TA. (b) Schematic illustration of surface functionalization process with cationic and zwitterionic polymer brushes onto SS substrate *via* "grafting-from" approach (reprinted with permission from ref. 96. Copyright © 2015, American Chemical Society).

(META), 2-methacryloyloxyethyl phosphorylcholine (MPC), and *N*-(3-sulfopropyl)-*N*-(methacryloxyethyl)-*N*,*N*-dimethylammonium betaine (SBMA) (Fig. 4b), the developed surfaces exhibited low WCA mainly due to the hydrophilic nature of polymer brushes. In a similar phenomenon, the TA-functionalized agarose (AgrTA) was prepared through the Williamson etherification of alkyl bromo moieties-modified Agr and TA. Direct adsorption and intermolecular oxidative crosslinking were used to deposit AgrTA onto Ti, SS, and silicon (Si) surfaces. It was established that the TA-inspired polymer deposition provided stable coatings that can endure varying pH (3–10) changes.[97]

To prepare a TA-anchored natural polymer-based antifouling surface, Xu *et al.*[44] have synthesized maleimide containing TA (TAMA) *via* etherification reaction using *N*-3-bromopropyl-maleimide (Fig. 5a). Further, the thiolated carboxymethyl chitosan (CMCSSH) was grafted onto TAMA-coated substrates through Michael addition reactions (Fig. 5b). It was disclosed that the addition of chain transfer agent (CTA) and azide moieties with TA resulted in the formation of 'clickable' macro-CTA (CTA–TA–N_3). Using the reversible addition–fragmentation chaintransfer (RAFT) polymerization, the zwitterionic poly(MPC) was grafted on CTA–TA–N_3 and CTA–TA. Subsequently, the dibenzocyclooctyne-ended and carbobenzoxyl groups-protected polylysine (DB-p(CbzLys)) were conjugated with p(MPC)–TA–N_3 *via* copper-free azide–alkyne 'click' reaction (Fig. 5c). After deprotection, TA-scaffold polymers can self-assemble onto different substrates with the aid of trihydroxyphenyl groups in TA. WCA measurements were used to evaluate the surface wettability of functionalized Si wafers. Interestingly, the WCA of Si–TA–p(MPC) surface was the smallest 21° as given in Fig. 5d, indicating the substantial hydration layer formation by the zwitterion p(MPC) brushes. A thick hydration layer acted as a barrier against micro-and macro-organism adhesion. Moreover, the surface hydrophilicity of Si–TA–p(MPC)/p(Lys) drops somewhat to a WCA of 23°, while Si–TA–p(Lys) had a small WCA of 29°. The coated surfaces showed reduced WCAs, highlighting its potential antifouling applications.[98] Besides, the azide-modified TA (TA–N_3) was demonstrated for its potentiality to construct a stimuli-responsive polymer-based coating with variable surface characteristics. The wettability of p(Lys) and poly(2-diisopropylaminoethyl methacrylate)-*b*-p(MPC) (p(DPA)-*b*-p(MPC)) mixed polymer brushes-modified Si surfaces (pH 7.4) was enhanced considerably with a small WCA of 32°, whereas their hydrophilicity was further increased at pH 5.5. After being treated with bacterial cells, the novel polymer coatings onto the SS surface showed improved antifouling and self-cleaning activities at pH 5.5. The fraction of dead bacterial cells was higher at pH 7.4, indicating the transition behavior of polymer at varying pH attributed to the switchable antimicrobial and antifouling functionalities.[59,99] Apart from the natural polymers, incorporating biocompatible non-immunogenic polymers like polyethylene glycol (PEG) with TA can be delivered as an effective antifouling surface. The assemblage of TA and four-armed PEG (PEG_{10k}-4-OH) onto Ti substrates has been carried out *via* a one-step or two-step process.[60,100]

Moreover, the TA-inspired assembly process has also been extended towards modifying polymeric substrates. Chen *et al.* used TA in conjunction with quaternized polyethylenimine (PEI-S) polymer to design a natural antifouling surface on various polymeric substrates. As given in Fig. 6a, the PEI or PEI-S was cross-linked with the pre-formed TA/Fe^{3+} complex in its oxidized state *via* the Schiff-base reaction or Michael-type addition. PEI–TA complexes have recently been shown to hold intrinsic benefits such as antifouling, antibacterial, and adhesive properties for durable coatings on a wide range of substrates using a one-step deposition technique.[101,102]

Likewise, the TA was employed as a cross-linker for engineering an implantable PP hernia mesh anchored with chondroitin sulfate and gelatin (CG) filament-anchored hydrogel layer (FAHL). The hydroxyl functional groups of TA were used to crosslink with polar groups of CG through various hydrophobic and hydrogen bonding interactions (Fig. 6b). The CG/TA-PP killed 99.99% of *Staphylococcus aureus* (*S. aureus*) but was least effective against Gram-negative bacteria. However, the mechanical characteristics of hydrogels were substantially influenced by the concentration of TA cross-linker and the treatment period (dipping time).[103] By utilizing TA as the non-covalent cross-linker,

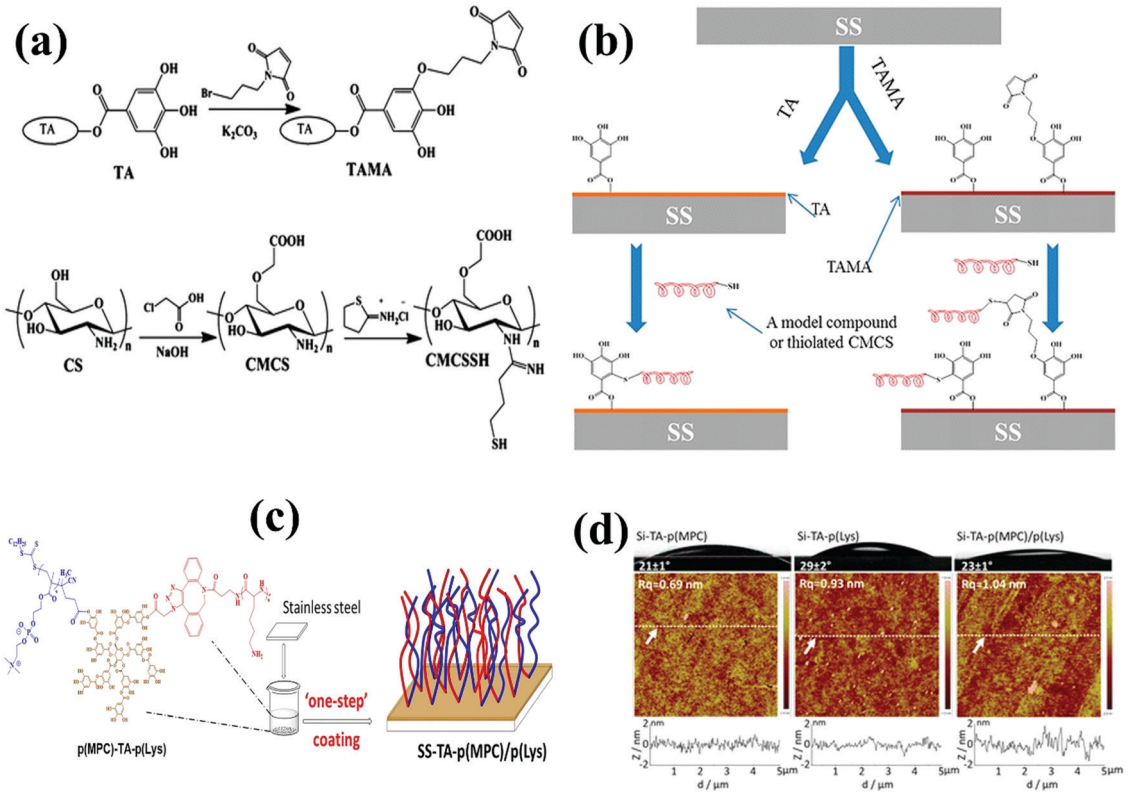

Fig. 5 (a) Synthesis of TAMA and CMCSSH. (b) Schematic of the TAMA preparation and anchoring on SS surface *via* bioinspired approach and subsequent functionalization with thiol-containing compounds *via* Michael addition (reprinted with permission from ref. 44. Copyright © 2016, American Chemical Society). (c) Schematic illustration of "One-Step" SS surface modification using TA-scaffolded polymer brush. (d) WCA photographs and AFM topography with cross-sectional height profiles of the Si–TA–p(Lys), Si–TA–p(MPC), and Si–TA–p(MPC)/p(Lys) surfaces (reprinted with permission from ref. 98. Copyright © 2019, American Chemical Society).

the resulting PEG–lysozyme (LZM)–TA hydrogel presented super toughness and high elasticity compared to the pristine PEG–LZM hydrogel (Fig. 6c). Notably, the increasing TA concentration densified the polymer network by releasing more than 50 wt% water from the PEG–LZM–TA hydrogel, eliminating the characteristic moisture and softness of hydrogel. The incorporation of TA elevated the deformability of hydrogel ten times 653 ± 45.4% (PEG–LZM–TA17) compared with the initial form 60.5 ± 7.2% (PEG–LZM). It was apparent that the TA concentration directly correlated with the formation of more non-covalent interactions within hydrogels and promoted the transition from elasticity to viscoelasticity.[104] Surgical sutures were the pivotal medical device to cure tendon injuries, decoration of porous tape sutures with chitosan/gelatin–TA (CS/GE–TA) offered anti-inflammatory and antimicrobial properties. After exposing the CS/GE-coated sutures in TA, the cross-linkage between CS/GE–TA was formed by hydrogen bond, Schiff base, and Michael addition reactions (Fig. 6d). The decoration of CS/GE–TA improved the hydrophilicity of sutures, which protected them from protein adsorption. Additionally, the porous tape sutures coated solely with CS/GE showed minimal antibacterial impact (14.29 ± 8.57% and 17.14 ± 4.13%) as compared with CS/GE–TA (95.10 ± 0.24% 84.57 ± 2.86%) against *S. aureus* and *Escherichia coli* (*E. coli*) respectively, confirming the active function of TA in antibacterial action and prevention of tendon-related infections.[105] Similarly, the monofilament suture was functionalized with the CS/GE–TA composite, followed by the *in situ* polymerization of polypyrrole (PPy). The CS–GE/TA/PPy composite-coated suture exhibited stable conductivity and superior antibacterial properties against *E. coli* and *S. aureus*. The electroactive and antibacterial suture significantly enhanced tissue regeneration under electrical stimulation.[106] The above-reported literature disclosed that the TA-polymer coating formulations benefited from improved physical, mechanical, and bioactivities. All these depictions were highly desired in clinical translation.

3.2. TA-Nanocomposite coatings

Generally, TA was used as a reducing/exfoliating agent, stabilizer, and fixation agent for the preparation and deposition of various inorganic nanomaterials, including metal,[107] metal oxides,[108] 2D nanomaterials,[109] carbon nanomaterials,[110] and their composites.[111] The TA-functionalized nanomaterials have gained specific interest simply because of their unique physiochemical features, stability, durability, and biocompatibility for clinical applications. Metal nanoparticles (MNPs) were formed by the redox reaction between TA and metal precursors (*e.g.*, Ag^{+} and Au^{3+}).[50,112] Due to the general surface binding affinity, the TA acted as a capping/stabilizing agent. At the same time,

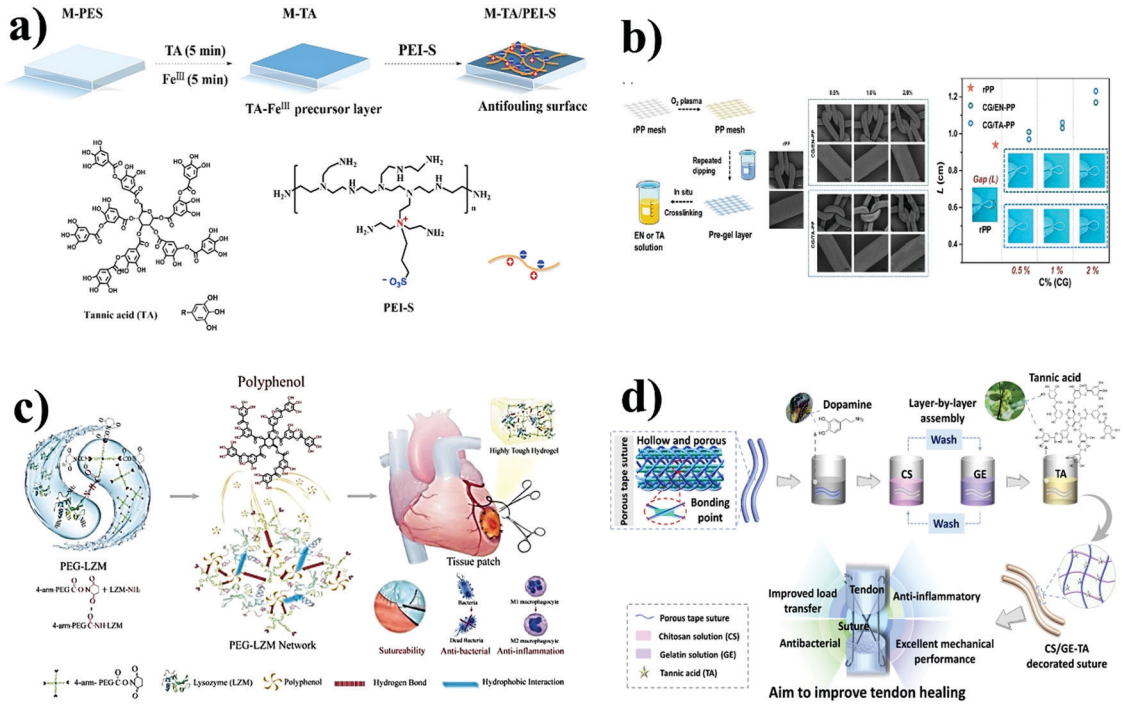

Fig. 6 (a) Schematic of antifouling polyethersulfone (PES) surface preparation *via* TA-inspired approach (reprinted with permission from ref. 102. Copyright © 2018, Elsevier). (b) The fabrication strategy of polypropylene (PP) hernia mesh with chondroitin sulfate and gelatin (CG) filament-anchored hydrogel layer (FAHL) and TA cross-linkers (reprinted with permission from ref. 103. Copyright © 2021, Elsevier). (c) Schematic of TA coupled PEG-lysozyme (LZM) hydrogel with features of suturability, anti-inflammation and antibacterial properties (reprinted with permission from ref. 104. Copyright © 2020, Royal Society of Chemistry) (d) Schematic of chitosan/gelatin-tannic acid (CS/GE-TA) decorated multifunctional suture fabrication process. (reprinted with permission from ref. 105. Copyright © 2021, Elsevier).

the end hydroxyl groups in TA could attach onto various substrates *via* a hydrogen bond, hydrophobic, metal coordination, and dynamic covalence formation.[85,113] The interaction and dispersion were related to multiple factors: (i) pH, (ii) content, and (iii) surface charge density.[114] The TA-nanocomposite coatings exhibited enhanced wettability and improved mechanical properties, offering antibacterial and antifouling activities with minimal toxic side effects.

The TA-functionalized MNPs and metal ions were coated by various methods such as drop-coating,[115] UV-assisted deposition,[85] self-assembly deposition[113] electrochemical coating,[116] and spray-coating.[117] Because of its outstanding and well-known antibacterial/antibiofilm characteristics, Ag has attracted much attention among the various MNPs. However, Ag's regenerative medicine uses are limited due to its excessive release from implants and dose-dependent cytotoxicity. The AgNPs coating with TA and biocompatible hydroxyapatite (HA) was proven to reduce harmful effects while preserving antibacterial activity (Fig. 7a). Immersion of titanium oxide nanotubes (TiO_2 NTs)-layered Ti substrates in the $AgNO_3$ (0.05, 0.1, and 0.2 M) and TA (10 g L^{-1}) solution mixtures resulted in the surface deposition of AgNPs. Remarkably, 0.1 M $AgNO_3$ showed homogeneous distribution along the surface with an average size of 50.73 ± 20.42 nm (Fig. 7b–j). The Ag–HA/TA composite coating exhibited potential antibacterial activity against *E. coli* and *S. aureus* after additional treatments with TA–$CaCl_2$ and Na_3PO_4 solutions to trigger the growth of bioactive needle-like HA (Fig. 7k–o).[116]

In the class of 2D nanomaterials, graphene oxide (GO) possesses unique physical, chemical, mechanical, and electrical properties.[118,119] The GO and its composite formulations have received immense attention in biomedical fields, including biosensor, imaging, drug/gene delivery, tissue engineering, regenerative medicine, and cancer theranostics due to their better biocompatibility.[120] Besides, utilizing GO as a potential bioactive material in regenerative and tissue engineering applications have recently surged in popularity, particularly for osteogenic differentiation. Furthermore, the sharp nano edge of graphene holds the ability to physically break bacterial integrity *via* penetrating and disrupting the cell membrane like a nano knife.[121,122] Li *et al.*[123] reported the fabrication of multilayer coating $(TA–GO/LZM)_n$ *via* the LbL technique for antibacterial and enhanced osteogenesis. UV-absorbance intensities confirmed the linear-dependent growth of LZM and TA–GO in the growth direction of $(TA–GO/LZM)_n$ coating. The multilayer growth was primarily mediated by TA–LZM interaction, which further functionalized onto GO-surface *via* π–π staking and hydrogen bonding. Physical properties of the coating morphology showed irregular island-shaped domains and outer layer-dependent stiffness. The $(TA–GO/LZM)_n$ coating effectively killed pathogenic bacteria and enhanced the osteogenic differentiation of human dental pulp stem cells (hDPSCs) due to the synergic effect.

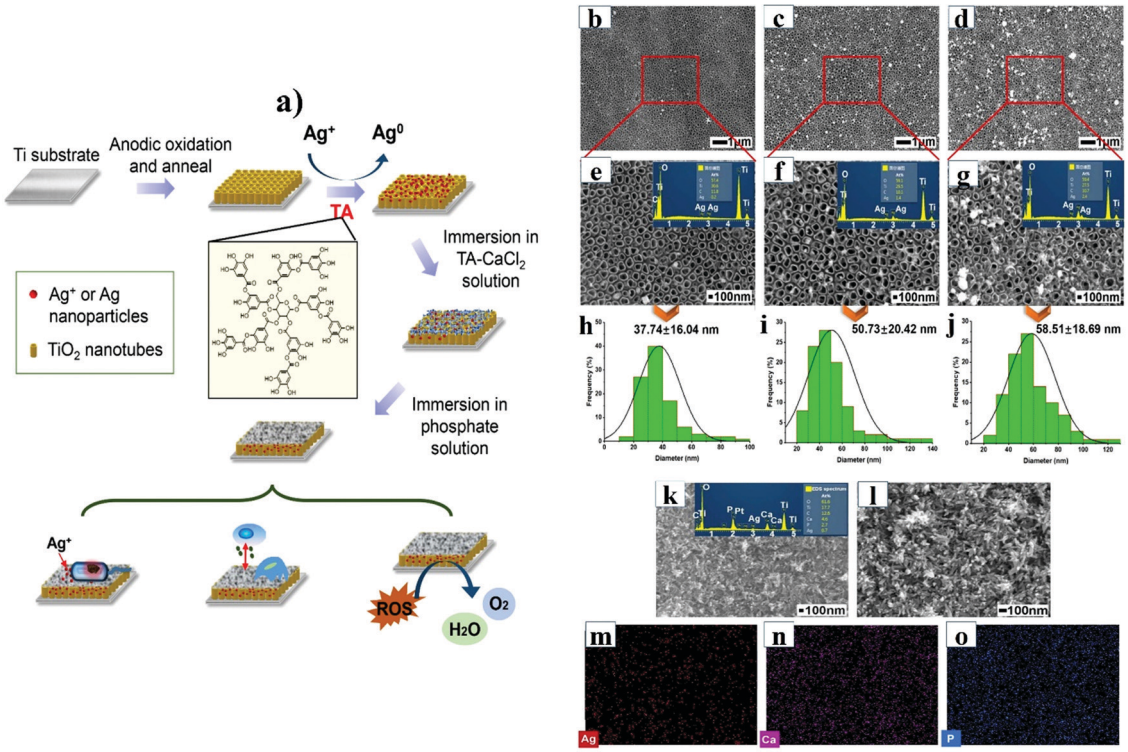

Fig. 7 (a) Schematic diagram of Ag–HA/TA composite coating formation based on the TiO_2 NTs arrays-layered Ti substrates. (b, e and h) SEM images, EDS spectra, and Ag nanoparticle diameter distributions of the samples after soaking in different concentrations of $AgNO_3$ solution and 10 g L^{-1} TA solution: 0.05 M $AgNO_3$, (c, f and i) 0.1 M $AgNO_3$, (d, g and j) 0.2 M $AgNO_3$. (k) SEM image with EDS spectrum and mapping elemental analysis: Ag (m), Ca (n) and P (o) of Ag–HA/TA-coated samples; A high magnification SEM image of Ag–HA/TA-coated samples (l) (reprinted with permission from ref. 116. Copyright © 2020, Elsevier).

Coating with the outermost layer of TA–GO was more significant than that with the outer deposited LZM. These films demonstrated the potential applicability on dental implant coatings by utilizing their potent antibacterial and osteogenic differentiation properties.

3.3. Metal ion–TA network coatings

Metal–phenolic networks (MPNs) are known for their versatility to fabricate surface coatings with better adhesive and mechanical properties. MPNs hold several benefits over other coatings, including the flexibility to modify surface thickness, chemical composition, and stability.[124] The abundant hydroxyl and gallol groups make TA a potential polydentate ligand or inorganic cross-linker for metal ions' chelation and coordination. For instance, Ejima *et al.*[49] established TA–Fe^{3+} complexes-based films at ambient temperature. Many research works have been undertaken to demonstrate the potential usage of TA–Fe^{3+} complexes in diverse applications, including surface modification, drug delivery, and imaging. Li *et al.* examined a universal process for depositing TA–Fe^{3+} complexes on polycaprolactone (PCL) nanofibers scaffolds for pre-vascularization applications.[125] The TA–Fe^{3+}/AgNPs-decorated Ti surfaces were formed by immersing the Ti substrates in the TA–Fe^{3+} solution mixture and ammoniacal silver solution successively (Fig. 8a).[126] The adhesive TA–Fe^{3+} complexes were co-deposited along with poly(*N*-isopropylacrylamide-*co*-SBMA) (p(NIPAM-*co*-SBMA)) microgels on Si substrate. As given in Fig. 8b, the dihydroxyphenyl group of TA enforced the micro gel assembly. The triple functionalities of thermo-responsive MPN-microgel coating have been validated with its excellent contact-killing of bacteria, antifouling, and self-cleaning properties.[127]

Likewise, a synergistic zipped-up TA–Fe^{3+}coating has been established with precise antioxidant and antifouling properties. The cyclic assembly of TA–Fe^{3+} (layer 1) consisting of noncovalent bonds retains the tendency to adsorb catechol side groups of dopamine-conjugated poly((MPC)-*co*-(acrylic acid)) (PMAD, layer 2), resulting in polyzwitterionic brushes formation on the PP surface *via* coordination and noncovalent bonds.[128] Other metal ions like Mg^{2+} were also selected to form the TA–Mg^{2+} complexes-based coating onto orthopedic implants. Increased loading mounts of Mg^{2+} were noticed in the multi-step process compared with one-pot assembly.[129] Recently, a facile method was demonstrated to deposit TA–Cu^{2+} (TA/Cu) complex and PEG chains hybrid film on medical substrates. For the hybrid film preparation, the TA/Cu complex layer (86.6 ± 1.0 nm) was first deposited on a gold surface (Au–TA/Cu) and subsequently immobilized with PEG outer layer (15.4 ± 3.0 nm). The inherent multifaceted features of the TA/Cu complex, such as immobilizer and photothermal conversion, offered significant antifouling and antibiofilm properties.[58]

3.4. Other TA-functional coatings

The long-term success of implanted materials mainly depends on their improved tissue integration and regeneration capabilities

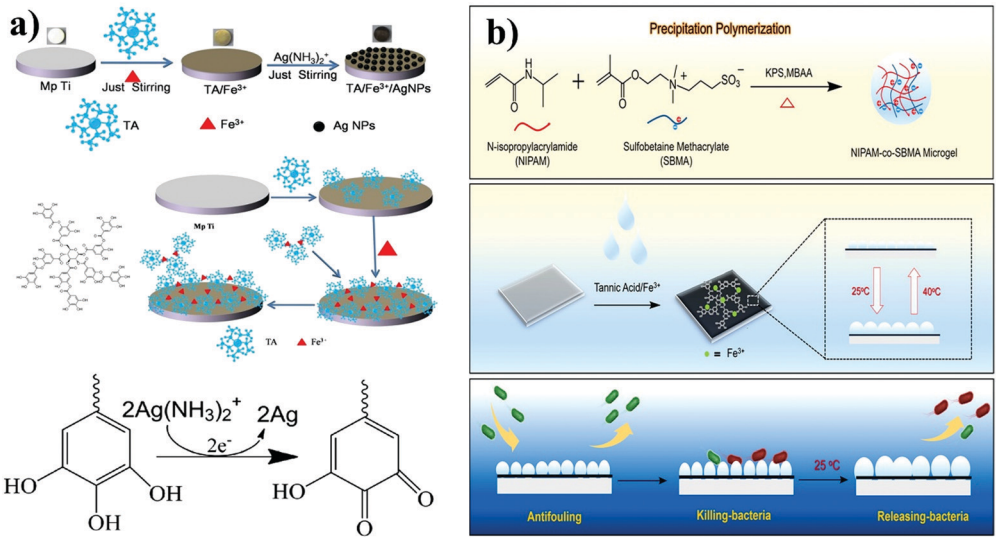

Fig. 8 (a) Schematic of the formation of TA–Fe^{3+}/AgNPs nanofilm on Ti implant *via* self-assembly and *in situ* reduction method (reproduced with permission from ref. 126. Copyright © 2017, American Chemical Society). (b) Schematic of the synthesis procedure of p(NIPAM-*co*-SBMA) microgel and one-step fabrication of the "antifouling-killing-releasing" multifunctional antibacterial coatings by TA–Fe^{3+} complexes and functional microgels. (reprinted with permission from ref. 127. Copyright © 2021, Elsevier).

with minimal risk of bacterial colonization. It has been demonstrated that incorporating active molecules such as HA, growth factors, peptides, minerals, and drugs into the implants can help ensure improved tissue regeneration.[130] HA is well known biocompatible osteoconductive apatite commonly used in bone implant coatings to improve the integration between implants and bone tissue. However, the pristine HA could not mimic natural bone due to several limitations like fracture toughness and abrasion resistance. To resolve these limitations, Ylmaz and co-workers designed and prepared a new implant coating comprising GO, COL, HA, and TA. The TA was found to have a pivotal role in promoting the deposition of HA–GO–COL coatings onto the TiO_2 NTs-layered Ti16Nb surfaces. TA was connected to GO *via* π–π interaction (GO–TA), resulting in HA modification for nucleation. Subsequently, the COL was attached to the aforementioned TA–HA–GO surface through hydrogen bond formation (biomimetic method).[131] A step further, versatile bioinspired coating with triple functions was achieved by integrating TA/LZM film, which gave a protective interface against deleterious impacts by ROS or bacteria and accelerated the healing process. Furthermore, the as-prepared TA/LZM showed a robust scavenging effect against overproduced ROS by its antioxidant ingredient TA. LZM improved the bacterial killing effect against *S. aureus*, *Micrococcus lysodeikticus* (*M. lysodeikticus*), and *E. coli via* damaging the cell membrane integrity.[132]

Most of the reported TA-based functional coatings are hydrophilic, which may not be suitable for the hydrophobic surfaces of several medical devices as it forms non-uniform structures. Under basic pH, the TA could be partially ionized and electrostatically assembled with cationic benzalkonium chloride (BAC) to form strongly hydrophobic (TBA) coatings on medical catheters. Compared with TA–Fe^{3+} complexes-based coating, the increased WCA of TBA depicted its hydrophobicity and stability of the prepared surface independent coatings. The TBA-coated thermoplastic polyurethane (TPU) surface exhibited an excellent bactericidal effect against catheter-associated infectious pathogens.[53] Similarly, Wang *et al.* devised a quaternary TA (QTA) for TPU catheter surface modification by combining dimethyl dodecyl 6-bromohexyl ammonium bromide (C12) and TA (Fig. 9a). Both *E. coli* and *S. aureus* showed that the concentration of QTA directly links with the percentage of antibacterial capabilities. At 0.10 mg cm^{-2} QTA, more than 90% of *S. aureus* died, and 0.20 mg cm^{-2} was needed to kill 80% of *E. coli* cells. In contrast to C12-embedded TPU, TPU–QTA contributed to very low QTA dissolution and leachability (0.345%).[133]

Our research team has disclosed that the amine moieties-integrated TA (TAA) can be used as a universal colorless coating platform to functionalize hydrophilic PEG brushes, biotin probes, and antibacterial AgNPs. As illustrated in Fig. 9b, the primary amine group was introduced onto the TA's galloyl moieties. Subsequently, the adhesion nature of TAA was exploited to deposit active components onto a variety of substrates, including PDMS, polystyrene (PS), Ti, SS, glass, and Si, using a simple immersion method under basic conditions. The TAA coating facilitated the grafting of PEG brushes onto the Au surface, resulting in increased protein repellency against bovine serum albumin (BSA) and fibrinogen (FBG) from human plasma. The TAA coating reduced Ag^+ ions, forming Ag NPs on the Ti surface. The resistance of Ti–TAA–AgNPs against *E. coli* and *S. aureus* was evidenced by the decreased cell numbers depicting its antibacterial and anti-adhesion properties.[134]

4. Biomedical perspective of TA coatings

4.1. Antibacterial/antibiofilm properties

Natural compounds such as plant polyphenols are being investigated as an alternative antibacterial agent to combat the

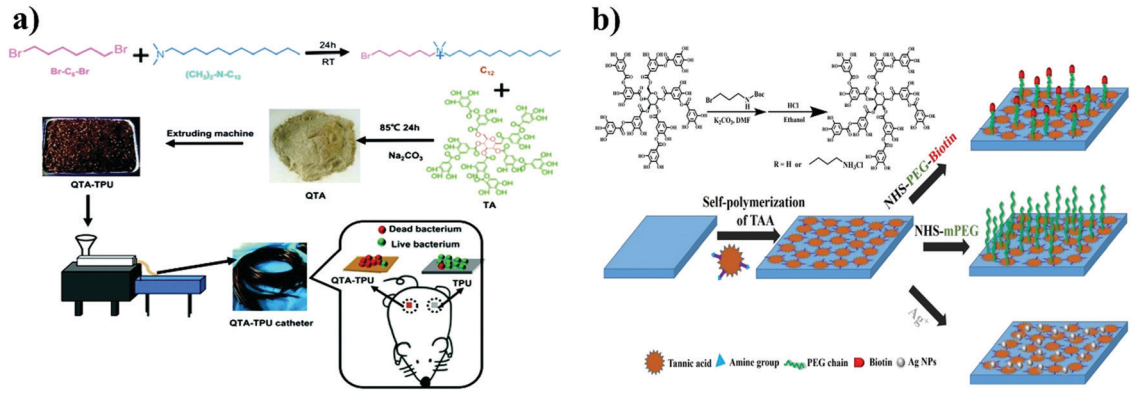

Fig. 9 (a) Schematic of TPU–QTA preparation and assessment of their biological properties (reprinted with permission from ref. 133. Copyright © 2021, Royal Society of Chemistry). (b) Schematic of TAA synthesis and deposition on the substrate surface for multiple functionalities (reprinted with permission from ref. 134. Copyright © 2020, Royal Society of Chemistry).

prevalence and emergence of MDR in bacteria.[135] Also, the differences in the cell wall structure of Gram-positive and Gram-negative bacteria demand a bioinspired universal antibacterial coating formulation that could trigger their cell membranes to collapse upon contact. Especially, the TA-engineered surfaces are being developed to combat IAI in tissue engineering and regenerative medicine. Therefore, understanding the basic information about bacterial killing or inhibitory actions of TA-engineered surfaces is crucial for designing and building viable surface coating strategies.[136]

4.1.1 Contact/Release killing surfaces. The colorless TA-modified polycarbonate surfaces displayed strong contact-based antibacterial effects against *Pseudomonas aeruginosa* (*P. aeruginosa*), and *S. aureus* after treatment for 3 h.[42] Formation of the hydrophilic coatings with specific stiffness tuned by pH and ionic strength inhibited bacterial adherence. At the same time, the contact-killing LbL films were constructed with positively charged moieties to attract negatively charged bacterial membranes *via* electrostatic attraction.[137] According to Meng's group, zwitterion moieties inhibited *E. coli* and *S. aureus* adhesion *via* forming a hydration layer and giving electrostatic shielding resistance.[84] Several release-killing LbL coatings have been developed to continuously release antibacterial compounds or metal ions by enzymatic degradation. However, the continuous discharge of antibacterial agents results in adverse side effects and the emergence of MDR bacteria. Therefore, it was necessary to develop stimuli-responsive coatings for the on-demand release of therapeutic agents to mitigate adverse side effects and premature depletion of the drug supply/reservoir. Many research works have recently been undertaken to formulate stimuli-responsive (ionic strength, temperature, and/or pH) LbL films that can discharge the payloads after applying external stimuli. Especially, the pH-responsive systems are largely formed by the self-assembly of neutral polymers and weak polyacids.[76] Most LbL assemblies are not sensitive to a critical pH window and decompose quickly, even at elevated pH. Also, the lower pH conditions of assembly may adversely affect the ability to integrate various sensitive therapeutics. TA-based LbL films were customized to obtain antifouling, anti-biofilm, and self-healing properties. Among these, the antibacterial properties of TA-based LbL films were achieved by incorporating antibacterial components. Kumorek *et al.* prepared a pH-responsive LbL film composed of CS or *N*-(2-hydroxypropyl)-3-trimethylammonium chitosan chloride (CMCH) in combination with TA to prevent bacterial infection. Turbid metric and surface plasmon resonance (SPR) analyses showed that the LbL films were formed at pH 5 and 7.4 through electrostatic interactions accompanied by hydrogen bonding.[138]

Another approach was established using a polymeric system-based localized drug discharge to overcome MDR and the toxic effects of antibiotics. For instance, integrating CS–PCL nanofibers on Ti–PDA (Ti–PDA/NF) surface by electrospinning bestowed a larger surface area and high cationic active sites. Further, the TA–antibiotic (Gentamicin sulphate, GS) multilayer was coated onto the Ti–NF surface (Ti–PDA/NF/LbL) using a standard LbL technique (dipping method) as given in Fig. 10a. The results also found that Ti–PDA/NF/LbL substrates released a higher GS than Ti/LbL substrates (Fig. 10b). Increased GS loading content of nanofiber than native Ti substrate was mainly because of its large surface area to volume ratio. Also, the Ti–PDA/NF/LbL surface improved antibacterial efficacy dramatically through increasing GS release at physiological pH (Fig. 10c and d).[139]

Further, the release of metal ions is well known for their broad spectrum of antibacterial properties, with no resistance reported so far. In a recent investigation, the nanocomposite coatings consisting of TA, graphene nanoplatelets (GNP), and Ag have displayed remarkable antibacterial/antibiofilm activities. The as-prepared GNP–TA–Ag@epoxy coating showed a synergistic antibacterial and antibiofilm activity with protecting the surface from bacterial adherence. Compared with the GNP–TA composite (256 μg mL^{-1}), the GNP–TA–Ag (64 μg mL^{-1}) exhibited improved inhibitory action against *E. coli* (50%) and *S. aureus* (80%), accrediting the active role of Ag in bacterial-killing. Furthermore, the TA and Ag were crucial in eliminating the bacteria upon contact with the surface, considering the bacterial-killing mechanism.[140]

After the immobilization on the PDMS surface, the Ag^+ release rate was found slow and exhibited long-term antibacterial

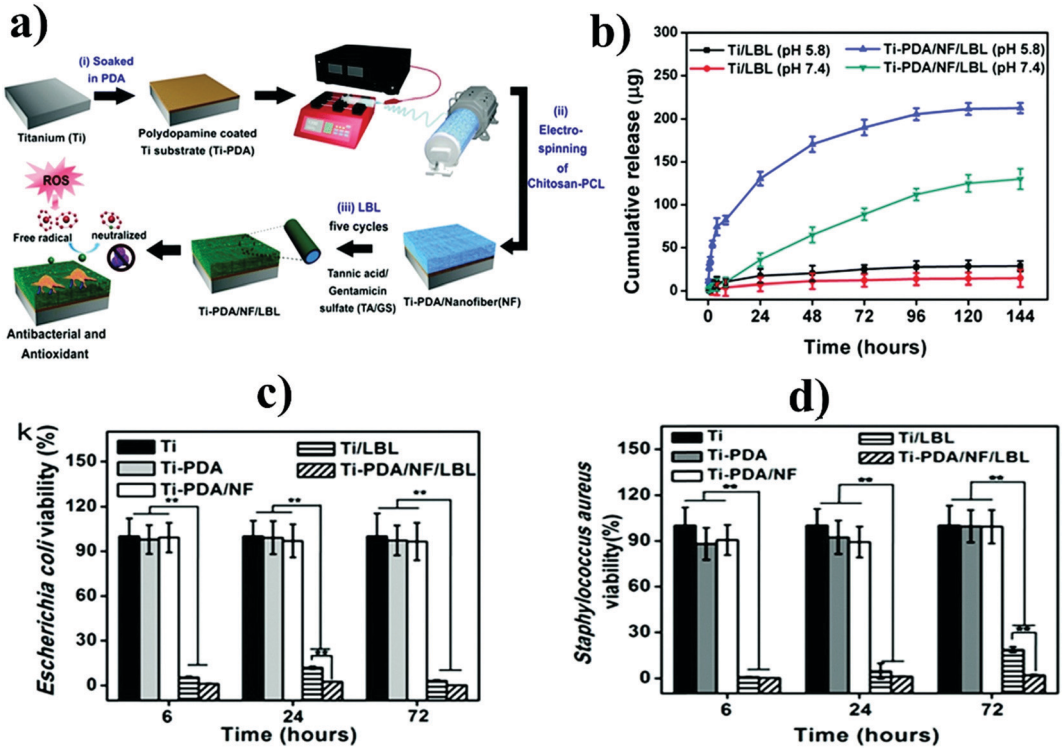

Fig. 10 (a) Schematic of Ti surface modification by CS-PCL electrospun nanofiber followed by multilayers of TA/GS through LbL methods. (b) Cumulative GS release profiles of Ti/LbL *vs.* Ti-PDA/NF/LbL on different pH. (c and d) *In vitro* quantitative antibacterial evaluation of different Ti surfaces against *E. coli* (c) and *S. aureus* (d) after 6, 24, and 72 h treatment (reprinted with permission from ref. 139. Copyright © 2018, Royal Society of Chemistry).

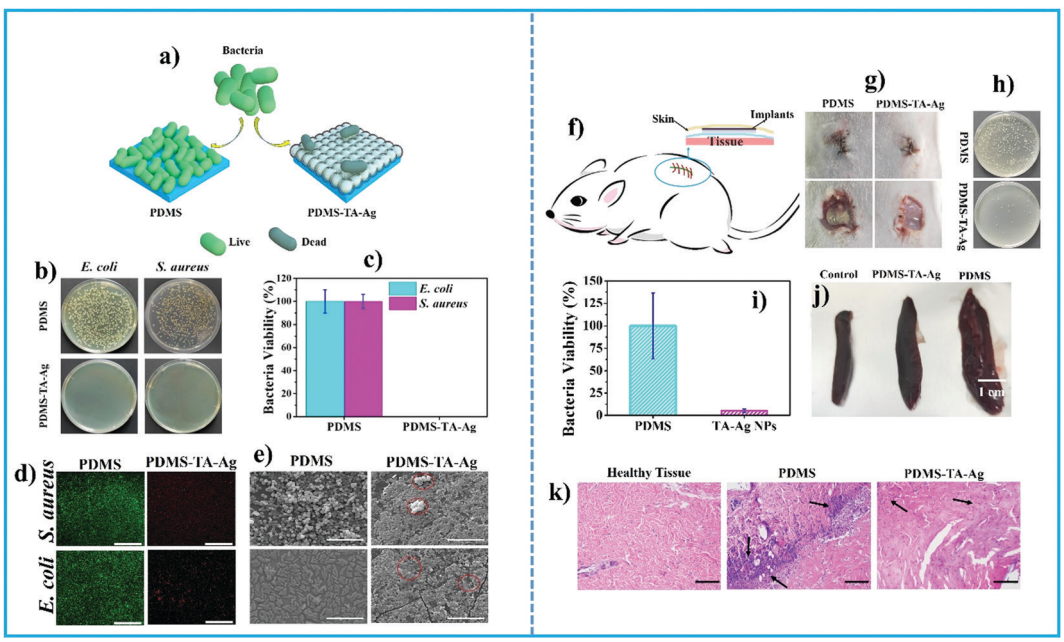

Fig. 11 (a) Schematic of antibacterial action of the PDMS–TA–Ag surface. (b) TSB–agar plates of *E. coli* and *S. aureus* detached from the pristine PDMS and PDMS–TA–Ag surfaces in the same dilution series. (c) Viability of bacteria on the pristine PDMS and PDMS–TA–Ag surfaces. The pristine PDMS and PDMS–TA–Ag surfaces were incubated with *E. coli* and *S. aureus* suspensions in 24-well plates for 4 h. (d) CLSM (scale bar = 100 μm) and (e) SEM (scale bar = 10 μm) images of adhered *E. coli* and *S. aureus* on the pristine PDMS and PDMS–TA–Ag surfaces. The pristine PDMS and PDMS–TA–Ag surfaces were cultured with *E. coli* and *S. aureus* suspensions with TSB for 24 h. (f) Illustration of the subcutaneous infection model; (g) photos of stitched and cut-off skins in contact with the pristine PDMS and PDMS–TA–Ag surfaces. (h) TSB–agar plates of *S. aureus* detached from the implanted PDMS and PDMS–TA–Ag surfaces at the same dilution series. (i) relative bacterial viability on the implanted PDMS and PDMS–TA–Ag surfaces (j) photo of spleens of the healthy rat and rats implanted with PDMS–TA–Ag and PDMS substrates. (k) H&E staining of the skins from the healthy rat and the pristine PDMS- and PDMS–TA–Ag implanted rats (scale bar = 100 μm) (reprinted with permission from ref. 85. Copyright © 2021, American Chemical Society).

action on a contact-killing basis (Fig. 11a). Due to the solid antibacterial property of Ag^+, the PDMS–TA–Ag surface showed improved bacterial inhibition, whereas the pristine PDMS surface did not show any activity against tested bacterial strains (Fig. 11b and c). As shown in Fig. 11d and e, the PDMS–TA–Ag surface inhibited bacterial adhesion and colonization. This functional coating strongly eradicated the adhered bacteria and prevented the biofilm formation of the drug-resistance pathogen. After the implantation, the PDMS–TA–Ag surface had a significantly lower bacterial infection and spleen inflammation level than the pristine PDMS surface (Fig. 11f–k).[85] It was also reported that the TA could destroy the integrity of peptidoglycan of the cell wall. On the other hand, the disassociation metal ions (Ag^+) leaching out from the surface holds the ability to target sulfur-containing biomolecules *via* cell membrane penetration.[141]

4.1.2 Photothermal killing. The adherence and colonization of planktonic bacterial pathogens on the inert surface of the implant were inevitable and caused severe issues in clinical applications. Although the diverse contact or release killing-based surface coating strategies were adequate, the continuous release of antibacterial components may promote the emergence of MDR strains and adverse side effects.[142–144] Hence, antibacterial photothermal therapy (aPTT)-based biofilm eradication routes have attracted much attention due to their minimally invasive, long-distance ablation, non-surgical, deep tissue penetration, and avoidance of MDR bacteria.[145] Diverse photo-absorbing inorganic nanomaterials such as metal,[146] carbon-based materials,[147] 2D nanomaterials,[148] and some photon-responsive polymeric systems[149] were developed to eliminate bacterial pathogens. Environmentally benign bioinspired universal coating technology is mandatory for the uniform deposition of photoactive materials onto various surfaces, including implants, hydrogels, scaffolds, and nanofibers.

As mentioned in the earlier sections, a plethora of contact or release-killing antibacterial surfaces has been reported. The main obstacle is most of the dead bacterial cells remain on the surface, which triggers undesirable immune and inflammatory responses. Chen's group developed innovative ''biocide-free'' bactericidal surfaces reinforced with photothermal agents for ''kill-and-release'' mechanism-based bacterial eradication to combat bacterial adherence and photo-killing (Fig. 12a and b). First, the TA–Fe^{3+} complexes were deposited onto the bare Au surface (Au–TA/Fe), followed by the surface grafting of PNIPAM chains (Au–TA/Fe–PNIPAM) *via* Schiff base reaction or Michael addition. The Au–TA/Fe and Au–TA/Fe–PNIPAM surfaces had good photothermal conversion efficiency (Fig. 12c and d).

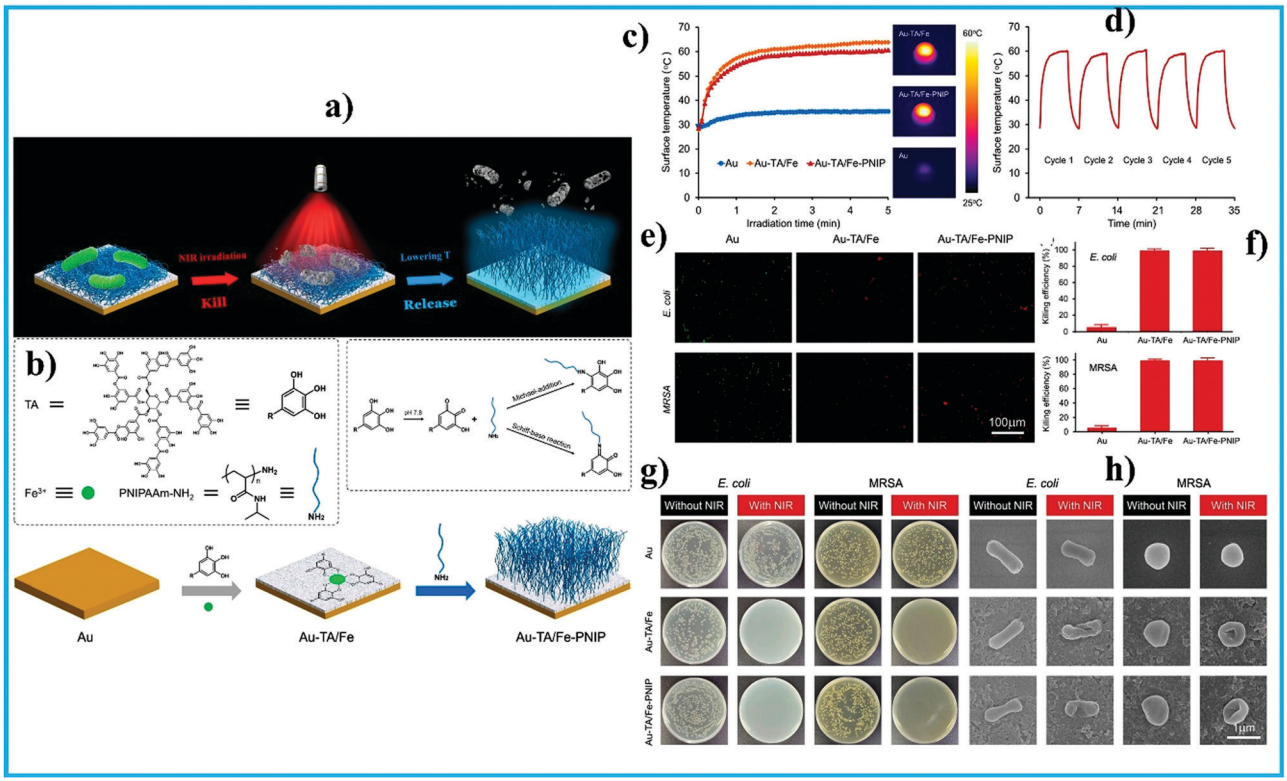

Fig. 12 (a) Schematic of photo-induced bacterial-killing and releasing functions (b) Schematic of the Au–TA/Fe–PNIPAM surface preparation. (c) Temperature variation of surfaces in PBS under NIR irradiation (2.2 W cm^{-2}). Corresponding thermal images are shown on the right. (d) on/off NIR irradiation (2.2 W cm^{-2})-triggered temperature change in Au–TA/Fe–PNIPAM surface over five cycles (e) Fluorescence images of live (green) and dead (red) bacterial pathogens (f) Corresponding killing efficiencies of the surfaces against *E. coli* and Methicillin-resistant *S. aureus* (MRSA). Data are mean ± SD (n = 3). (g) Representative agar-plate photographs of bacterial (*E. coli* or MRSA) colonies formed after being disassociated from various surfaces and (h) SEM images of attached bacteria (*E. coli* or MRSA) on different surfaces with/without NIR irradiation (2.2 W cm^{-2}, 5 min) (reprinted with permission from ref. 150. Copyright © 2020, American Chemical Society).

More than 99% of bacterial cells attached to the Au–TA/Fe and Au–TA/Fe–PNIPAM surfaces emitted red fluorescence, assigning the bacterial cell death *via* NIR-induced hyperthermia (Fig. 12e and f). SEM micrographs of attached bacteria without NIR irradiation showed intact cell membrane structure, whereas 5 min NIR irradiation triggered shrinkage and bacterial membrane depletion on Au–TA/Fe and Au–TA/Fe–PNIPAM surfaces (Fig. 12h). Moreover, due to the thermoresponsive properties of the grafted PNIPAM, all of the dead bacterial debris on the surface was cleansed by regulating the temperature (Fig. 12g).[150]

Adopting a similar phenomenon, our group has designed and developed a passive eco-friendly coating strategy for solid surfaces. The TA-functionalized Au NPs were deposited along with PEG onto the PDMS substrate *via* one-step assembly. Upon 808 nm laser irradiation, the increasing temperature of PDMS–TA–PEG–Au surface (~90 °C) compared to pristine PDMS (~45 °C) and PDMS–TA–Au (~53 °C) signified its improved and stable photo-killing effect for repeated cycles. Subcutaneous implantation of the prepared substrate with *S. aureus* inoculation and NIR irradiation eliminated the bacterial adhesion and bestowed suitable conditions for aPTT.[113]

Recently, the solid antifouling property of PEG was shown to resist the adherence and colonization of planktonic bacteria on TA/Cu complex coated Au surface. Upon short NIR irradiation, the TA/Cu complex efficiently killed *S. aureus* and prevented Au surface from biofilm formation for a prolonged period (15 days). In the extended *in vivo* studies, pristine polyurethane (PU) and PU-TA/Cu-PEG surfaces were incubated with *S. aureus* before implanting on rat incision models (Fig. 13a). After the implantation and NIR irradiation (1 W cm^{-2}, 5 min), the PU-TA/Cu-PEG surface exhibited 1.2, 3.4, and 2.0 log reduction of bacterial colonies at 1, 4, and 11 days comparatively with unmodified PU surface (Fig. 13b). On the other hand, the negligible inflammatory response of PU–TA/Cu–PEG (Fig. 13c) validated its potential in combating IAI of biomaterials and devices.[58]

4.1.3 Photodynamic therapy. Antibacterial photodynamic therapy (aPDT) is a non-systemic therapeutic venture that uses laser irradiation and molecular oxygen to kill germs.[9] In general, three essential prerequisites for APDT are PS's, light sources, and molecular oxygen. Combining these three elements in optimized proportions turns on cascades of reactions and gives improved bacterial killing effect, especially against MDR bacteria.[151,152] The APDT can be used even after surgery, chemotherapy, and radiotherapy without inducing any immunosuppressive or myelosuppressive effects. The sustained release of metal ions from active nanocoatings on implant surface reduces IAI and other

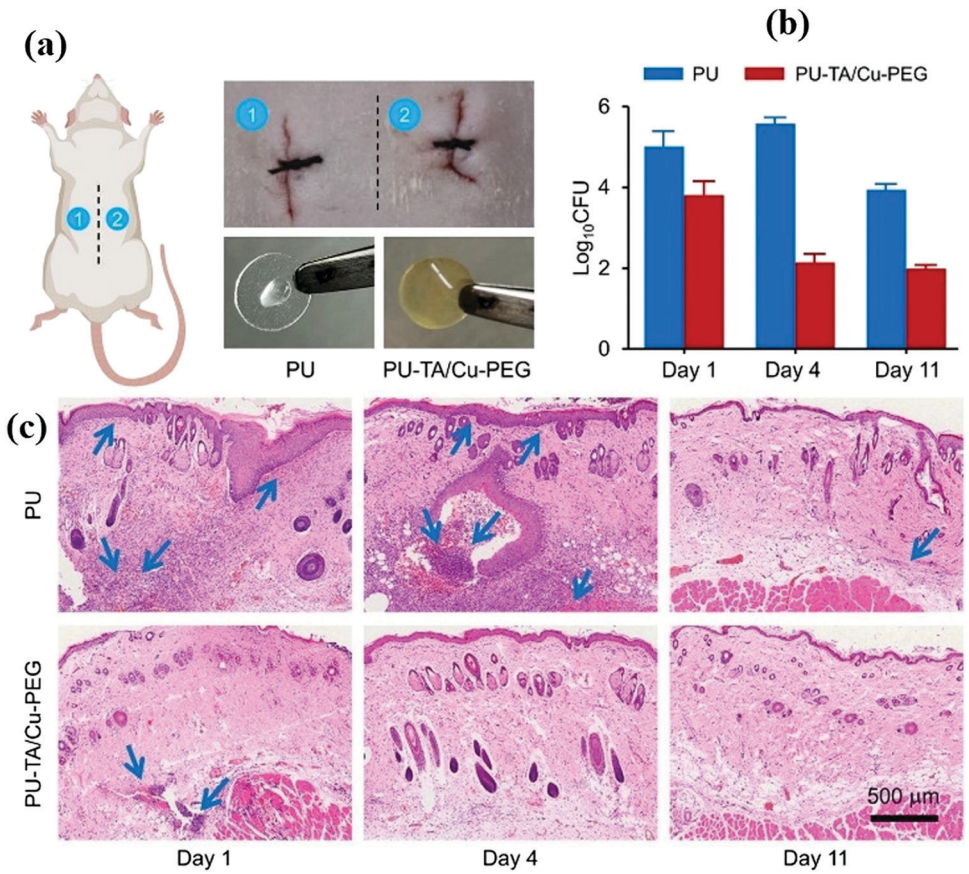

Fig. 13 (a) Schematic of *in vivo* rat model used for testing antibacterial property of bacteria-contaminated surfaces. (b) Bacterial colonies of PU and PU–TA/Cu–PEG surfaces after implantation for 1, 4, and 11 days. Data are mean ± SD (n = 3). (c) After implantation, histological sections of surrounding tissues for 1, 4, and 11 days (Blue arrows represent neutrophils) (reprinted with permission from ref. 58. Copyright © 2021, American Chemical Society).

infectious risk factors, including bacteria, fungi, and other microbes, with minimal toxicity. It has also been discovered that plasmonic excitation of metallic nanostructures (*e.g.*, Au, Ag, and Pt) produces singlet oxygen ($^1O_2$), which is significant in microbe death.[153] Under light irradiation, Ag NPs can kill bacteria by producing $^1O_2$, a process known as photodynamic inactivation (PDI) (Fig. 14a). Only a few research works have been reported so far on the polyphenol-based coatings for aPDT, most likely because of hindrance in $^1O_2$ or ROS generation by the active polyphenols. Xu *et al.* have proven that the Ag NPs-anchored TA–Fe^{3+} complexes coatings released Ag^+ ions for the long term (5–30 days). The efficiency of TA–Fe^{3+} complexes/AgNPs-5 (prepared from 5 mM ammoniacal silver solution) against *E. coli* and *S. aureus* was about 83 and 60%, respectively, but the comparable efficiency of TA–Fe^{3+} complexes/AgNPs-10 (prepared from 10 mM ammoniacal silver solution) improved to 100 and 90%. Interestingly, the high PDI action could be attributed to the increased Ag^+ release and oxidative stress-mediated bacterial cell death (Fig. 14b–f).[126]

4.2. Antifouling applications

Antifouling surfaces coating strategies are becoming prominent in the healthcare industry to protect biomedical devices from micro-and macro-fouling agents.[154] More specifically, the protein adsorption on the implant surface minimizes their sensitivity and leads to failure and other adverse side effects. TA has been used as a building block to fabricate bioinspired hydrophilic surfaces *via* incorporating various functional materials.[44,96–100,102] The anti-biofouling ability of the super-hydrophilic surface can be explained using water layer theory.

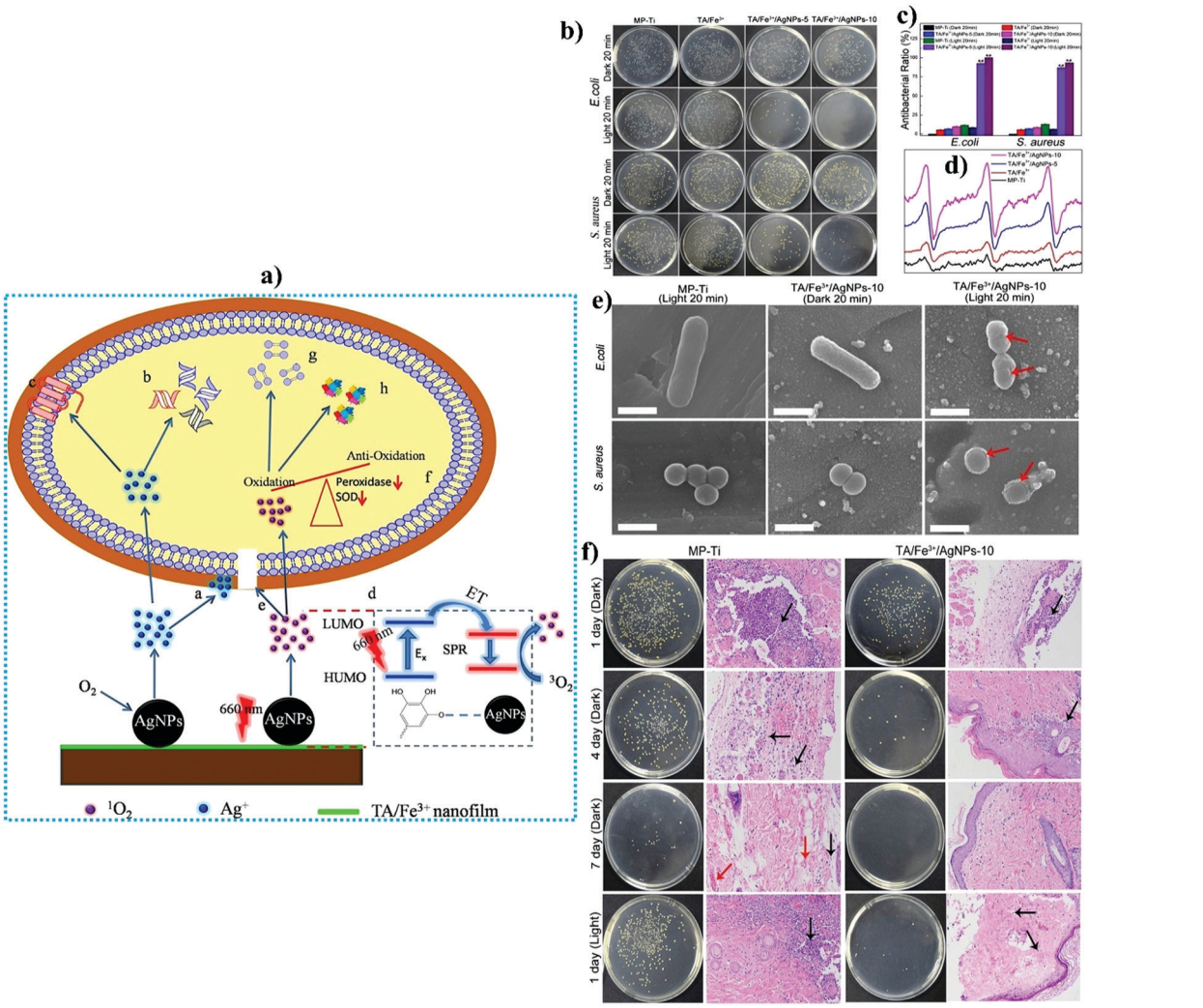

Fig. 14 (a) Schematic of the APDT mechanism of TA–Fe^{3+} complexes/AgNPs. (b) Plate photographs showing *E. coli* and *S. aureus* colonies after incubation with different samples under the illumination of 660 nm visible light for 20 min or in the dark. (c) Antibacterial ratio of different samples quantified based on the number of colonies visible in the plate samples $^{**}P < 0.01$ *vs.* the Ti group as the control. (d) ESR signals of $^1O_2$ were obtained upon irradiation of different samples for 20 min in the presence of ROS trap. (e) Morphological features of *E. coli* and *S. aureus* treated on the Ti and Ti–TA–Fe^{3+} complexes/AgNPs surfaces under the illumination of 660 nm visible light for 20 min. (f) Plates showing *S. aureus* colonies collected from the subcutaneous infection model and corresponding H&E stained histological sections of tissues adherent to different samples (reprinted with permission from ref. 126. Copyright © 2017, American Chemical Society).

A dense coating of water molecules on super-hydrophilic surfaces inhibits bacteria or protein adhesion by weakening the interface between substrate and fouler. For example, the CMCS modified-SS surface exhibited better anti-nonspecific protein adsorption performance in our earlier study, whereas the SS and SS–TAMA surface readily adsorbed BSA.[44] In addition, zwitterion compounds with a positive and negative electrical charge in close proximity can coat material surfaces to limit non-specific protein adsorption and biofilm formation. Yang *et al.* constructed a super-hydrophilic surface to resist protein adsorption by preparing the DDDEEKC peptide-modified TA (SAP3-TA). The hydrophilic surface can prevent the absorption of BSA and further inhibit the adhesion of *Streptococcus mutans* (*S. mutans*).[130] We have recently utilized the hydrophilic silk

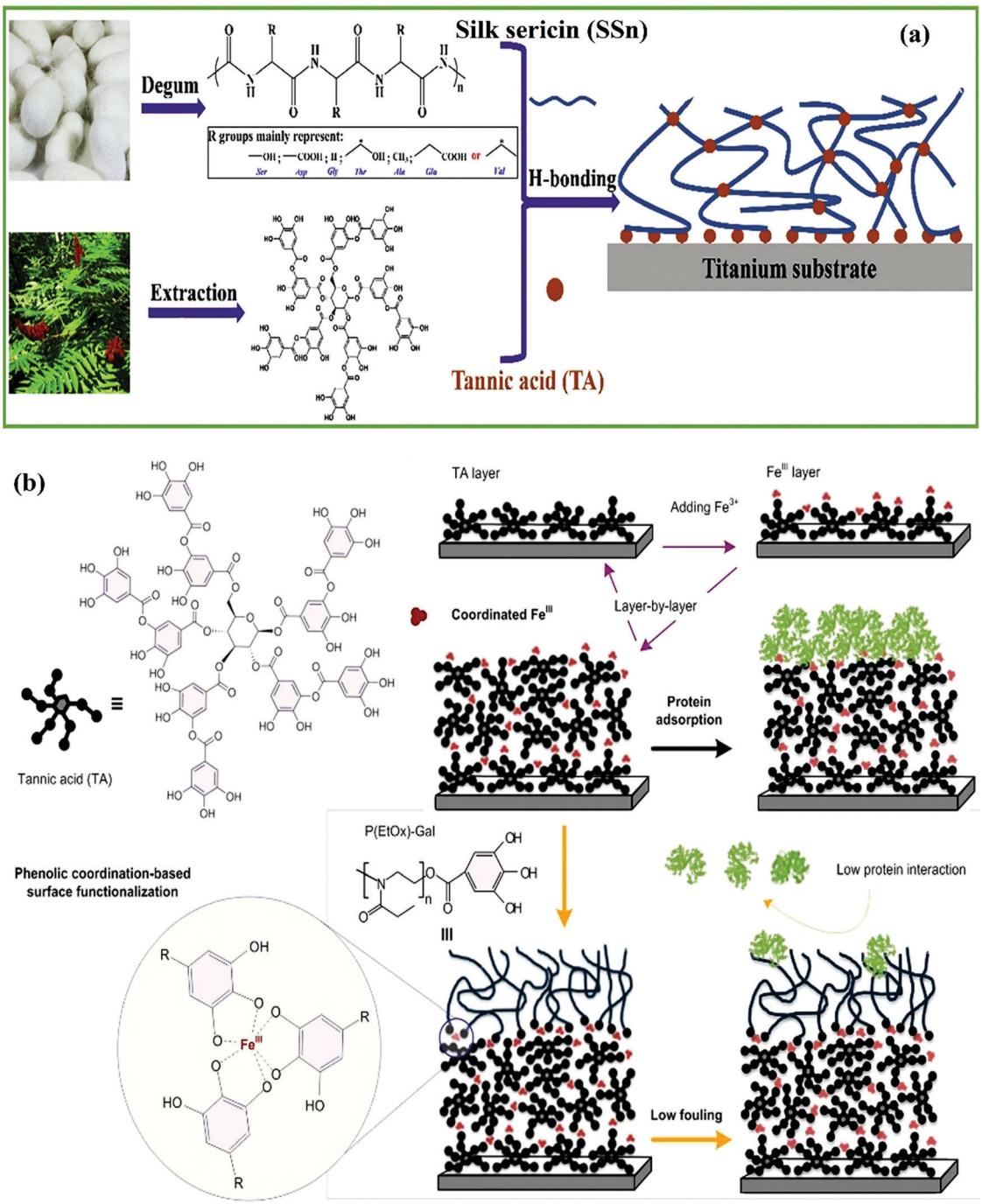

Fig. 15 (a) Schematic illustration for the fabrication of antifouling coating on the Ti surface using natural TA and biocompatible SSn (reprinted with permission from ref. 155. Copyright © 2020, Elsevier) (b) Schematic of TA–Fe^{3+} LbL assembly process and subsequent fouling on non-functionalized (pristine) and P(EtOx)-Gal functionalized films for antifouling applications (reprinted with permission from ref. 156. Copyright © 2019, American Chemical Society).

sericin (SSn)-conjugated TA as a value-added product to protect the implant from fouling effects. The BSA and FBG adsorbed on the bare Au chips were quantified to be 3.39 ± 0.37 and 7.67 ± 0.13 ng mm^{-2}, respectively. After TA functionalization, the adsorbing rate of BSA and FBG on the sensing surfaces decreased slightly (2.83 ± 0.33 and 6.10 ± 0.46 ng mm^{-2}) due to hydrogen bonding interactions between TA and proteins (Fig. 15a).[155] Similarly, the TA–PEG assembly on the Ti surface also exhibited remarkable antiadhesive and antifouling properties. The better protein repellency of TA–PEG coating was mainly because of the robust inhibitory ability of PEG towards non-specific protein adsorption.[100]

Interestingly, the grafting of galloyl-modified poly(2-ethyl-2-oxazoline) (P(EtOx)–Gal) to the TA–Fe^{3+} films *via* coordination bonds deliver effective surface modification strategies to minimize biofouling effects (Fig. 15b). Furthermore, the quantitative measurements demonstrated that the P(EtOx)-Gal-functionalized TA–Fe^{3+} films showed maximum reduction ($\sim$2.5 mg m^{-2}) of BSA, immunoglobulin G (IgG), and FBG adhesion compared to pristine TA–Fe^{3+} film.[156] An earlier study suggested that the TA-functionalized surfaces with excessive galloyl could adsorb FBG *via* bonding, electrostatic and hydrophobic interactions. Later, the strong interaction between the galloyl groups and FBG triggered the inactivation of α and γ chains of the adsorbed FBG, which ultimately bestowed remarkable antiplatelet adhesion surfaces. Collectively, the TA-based surface coating strategies can be successfully applied to construct new-generation blood-contacting bioactive materials.[157] Overall, the TA-based surface engineering strategies possess many biomedical advantages, as given below

- The incorporation of bioactive polyphenol TA bestows augmented the antibacterial and antibiofilm efficiency against MDR pathogens.
- The increased adhesiveness of TA-modified implant substrates provides an effective platform for cellular attachment, tissue integration, and regeneration.
- Improved hydrophilicity may reduce the adherence of fouling agents and protect medical devices from blood–protein absorption.
- The inherent biocompatibility of TA-modified biomedical implants represents a broad spectrum of tissue engineering and regenerative medicine applications.

5. Conclusions and future prospects

In this review, we focused on the various standard and recent bioinspired surface coating techniques that have been used to deposit TA in combination with active payloads. Also, the involvement of different physiochemical interactions like hydrogen bonds, hydrophobic interactions, electrostatic interactions, polyphenol–metal coordination compounds, and Michael addition/Schiff base reactions and their role in TA coating onto substrate were given elaborately. However, a better understanding of the TA or TA/Fe^{3+} interactions with different substrates is mandatory due to TA's complex chemical structure, resulting in more than one bonding formation. Therefore, more theoretical calculations can be adopted to elucidate the specific interactions between TA and substrates to attain universal substrate-independent coating technology with a scaled-up process.

Considering all the distinct surface modification strategies, the deposition process is determined by the materials or active molecules used and the substrate type. In the LbL method, the film's composition, architecture, thickness, and mechanical characteristics can be controlled *via* changing the assembly conditions. The LbL assembly technique has been adopted to tether and release various antibiotics, polymers, biomolecules, and nanomaterials. As recent progress, the electrophoretic and UV-assisted deposition methods have also been explored to develop TA-based surface modifications. Compared with the LbL-based techniques, these advanced deposition routes offer rapid and uniform coating of polymers and nanomaterials with improved properties. In particular, the UV-assisted method actively improves the redox reaction of TA with metal ions and the simultaneous deposition of monodispersed nanoparticles onto the substrate. Also, different parameters such as optimizing the light dosage, irradiation time, and other reaction kinetics deliver an effective protocol for the fabrication of nanocoating with different structures and functionalities.

Several natural and synthetic polymeric materials have been investigated as a framework for developing a contact or release killing surface with hydrophilic nature to prevent fouling and biofilm formation. Especially, the coatings reinforced with natural polymer provide excellent compatibility for clinical applications. In addition, TA considerably boosted the coating's stability because of its involvement in noncovalent interactions and hydrogen bonding. The stimuli-responsive or controlled release polymeric coating formulations serve as delivery systems to deliver antibiotics or metal ions on bacterial contamination in a controlled release manner. Likewise, the nanomaterials and other active components were also exploited in TA-based coating technology for rapid tissue integration and other medical purposes. Each coating formulations have a specific function to protect the biomaterials from fouling agents and bacterial pathogens. As a result, nanomaterials modified implants, scaffolds, and hydrogels offering advanced phototherapeutic ventures for remote eradication of bacterial pathogens with less operational risks. Incorporation of other essential ingredients like minerals, proteins, and biomolecules can also be used for surface modification of various biomedical implants.

Last but not least, because of its inherent antibacterial and adhesive quality, TA is a good building block for the bioinspired universal coating of various implantable substrates and medical devices. Antibacterial, antibiofilm, antifouling, and self-cleaning capabilities of TA-tethered with polymer, nanomaterials, and other active compounds were reported to be promising. The use of TA opens up new possibilities for bacterial treatments in all terms of approach, including contact killing, drug release, and PTT/PDT representing a viable opportunity to minimize the risks of MDR bacterial emergence. Based on the rapid advancements in bioinspired surface coating technology, more research will inevitably be devoted toward

identifying innovative functional materials-based coatings with more diversified and tailored architectures. In most of the reported TA-based coatings, the TA bestowed strong biocompatibility and showed only negligible or no sign of toxicity compared with TA-free coatings. However, all-inclusive preclinical trials are required to validate engineered materials' efficacy and toxicity implications for biomedical purposes. This review provides insight into recent research focused on TA-based functional coatings to treat IAI. We believe that a facile, cost-effective, and eco-friendly bioinspired universal coating technology will soon be available to treat bacterial infections in the medical field with extensive future research investigations.

Conflicts of interest

There are no conflicts to declare.

Acknowledgements

This research was supported by the National Natural Science Foundation of China (21504072, 51741304 and 52073234), Natural Science Foundation of Chongqing (cstc2019jcyj-msxmX0363 and cstc2021jcyj-msxmX0513), Sichuan Science and Technology Program (2021JDRC0102), Innovation Teams in Colleges and Universities of Chongqing (CXQT20005), the innovation platform for Academicians of Hainan Province and Chongqing Engineering Research Center for Micro-Nano Biomedical Materials and Devices.

References

1 R. Darouiche, *N. Eng J. Med.*, 2004, **351**, 194–195.
2 K. G. Neoh, X. Hu, D. Zheng and E. T. Kang, *Biomaterials*, 2012, **33**, 2813–2822.
3 C. R. Arciola, D. Campoccia and L. Montanaro, *Nat. Rev. Microbiol.*, 2018, **16**, 397–409.
4 G. Bixler and B. Bhushan, *Philos. Trans. R. Soc., A*, 2012, **370**, 2381–2417.
5 Y. Dhar and Y. Han, *Eng. Regen.*, 2020, **1**, 64–75.
6 L. A. Mermel, B. M. Farr, R. J. Sherertz, I. I. Raad, N. O'Grady, J. S. Harris and D. E. Craven, *Infect. Control Hosp. Epidemiol.*, 2001, **22**, 222–242.
7 D. Campoccia, L. Montanaro and C. R. Arciola, *Biomaterials*, 2006, **27**, 2331–2339.
8 T. Wang, C. Wang, S. Zhou, J. Xu, W. Jiang, L. Tan and J. Fu, *Chem. Mater.*, 2017, **29**, 8325–8337.
9 Q. Jia, Q. Song, P. Li and W. Huang, *Adv. Healthcare Mater.*, 2019, **8**, 1900608.
10 H. Yazici, M. B. O'Neill, T. Kacar, B. R. Wilson, E. E. Oren, M. Sarikaya and C. Tamerler, *ACS Appl. Mater. Interfaces*, 2016, **8**, 5070–5081.
11 A. Sobolev, A. Valkov, A. Kossenko, I. Wolicki, M. Zinigrad and K. Borodianskiy, *ACS Appl. Mater. Interfaces*, 2019, **11**, 39534–39544.
12 L. Zhang, C. Ning, T. Zhou, X. Liu, K. Yeung, T. Zhang, Z. Xu, X. Wang, S. Wu and P. K. Chu, *ACS Appl. Mater. Interfaces*, 2014, **6**, 17323–17345.
13 Q. Gao, T. Feng, D. Huang, P. Liu, P. Lin, Y. Wu, Z. Ye, J. Ji, P. Li and W. Huang, *Biomater. Sci.*, 2020, **8**, 278–289.
14 N. N. Ashton, G. Allyn, S. T. Porter, T. J. Haussener, P. R. Sebahar, R. E. Looper and D. L. Williams, *Acta Biomater.*, 2019, **93**, 25–35.
15 B. Wang, T. Jin, Q. Xu, H. Liu, Z. Ye and H. Chen, *Bioconjugate Chem.*, 2016, **27**, 1305–1313.
16 P. Ducheyne, W. Van Raemdonck, J. Heughebaert and M. Heughebaert, *Biomaterials*, 1986, **7**, 97–103.
17 M. Đošić, S. Eraković, A. Janković, M. Vukašinović-Sekulić, I. Z. Matić, J. Stojanović, K. Y. Rhee, V. Mišković-Stanković and S.-J. Park, *J. Ind. Eng. Chem.*, 2017, **47**, 336–347.
18 M. Stevanovic, M. Dosic, A. Jankovic, V. Kojic, M. Vukasinovic-Sekulic, J. Stojanovic, J. Odovic, M. Crevar Sakac, K. Y. Rhee and V. Miskovic-Stankovic, *ACS Biomater. Sci. Eng.*, 2018, **4**, 3994–4007.
19 R. Drevet, Y. Zhukova, S. Dubinskiy, A. Kazakbiev, V. Naumenko, M. Abakumov, J. Fauré, H. Benhayoune and S. Prokoshkin, *J. Alloys Compd.*, 2019, **793**, 576–582.
20 X. Mi, M. J. Gupte, Z. Zhang, W. B. Swanson, L. K. McCauley and P. X. Ma, *ACS Appl. Mater. Interfaces*, 2020, **12**, 32503–32513.
21 J. Jansen, J. Wolke, S. Swann, J. Van Der Waerden and K. De Groof, *Clin. Oral. Implants Res.*, 1993, **4**, 28–34.
22 H.-J. Jian, J. Yu, Y.-J. Li, B. Unnikrishnan, Y.-F. Huang, L.-J. Luo, D. H.-K. Ma, S. G. Harroun, H.-T. Chang and H.-J. Lin, *Chem. Eng. J.*, 2020, **386**, 123913.
23 M. Li, L. Li, K. Su, X. Liu, T. Zhang, Y. Liang, D. Jing, X. Yang, D. Zheng and Z. Cui, *Adv. Sci.*, 2019, **6**, 1900599.
24 R. Shi, J. Zhang, J. Tian, C. Zhao, Z. Li, Y. Zhang, Y. Li, C. Wu, W. Tian and Z. Li, *Nano Energy*, 2020, **77**, 105201.
25 B. Stuart, G. Stan, A. Popa, M. Carrington, I. Zgura, M. Necsulescu and D. Grant, *Bioact. Mater.*, 2022, **8**, 325–340.
26 J. Henao, C. Poblano-Salas, M. Monsalve, J. Corona-Castuera and O. Barceinas-Sanchez, *J. Mater. Res. Technol.*, 2019, **8**, 4965–4984.
27 M. Chen, H. Li, X. Wang, G. Qin and E. Zhang, *Appl. Surf. Sci.*, 2019, **463**, 261–274.
28 A. Khlyustova, Y. Cheng and R. Yang, *J. Mater. Chem. B*, 2020, **8**, 6588–6609.
29 J. G. Souza, M. Bertolini, R. C. Costa, J. M. Cordeiro, B. E. Nagay, A. B. De Almeida, B. Retamal-Valdes, F. H. Nociti, M. Feres and E. C. Rangel, *ACS Appl. Mater. Interfaces*, 2020, **12**, 10118–10129.
30 G. Popescu-Pelin, C. Ristoscu, L. Duta, G. E. Stan, I. Pasuk, T. Tite, M. S. Stan, C. Bleotu, M. Popa and M. C. Chifiriuc, *ACS Sustainable Chem. Eng.*, 2020, **8**, 4026–4036.
31 W. Jin and P. K. Chu, *Surf. Coat. Technol.*, 2018, **336**, 2–8.
32 Y. Su, Z. Zhi, Q. Gao, M. Xie, M. Yu, B. Lei, P. Li and P. X. Ma, *Adv. Healthcare Mater.*, 2017, **6**, 1601173.
33 A. K. Muszanska, H. J. Busscher, A. Herrmann, H. C. van der Mei and W. Norde, *Biomaterials*, 2011, **32**, 6333–6341.

34 S. Yang, Y. Xu, Q. Lin, Y. Bai, X. Zan and Q. Ye, *Chem. Commun.*, 2019, **55**, 2058–2061.
35 H. Xu, Y. Cai, X. Chu, H. Chu, J. Li and D. Zhang, *Polym. Chem.*, 2021, **12**, 3413–3426.
36 H. Lee, S. M. Dellatore, W. M. Miller and P. B. Messersmith, *Science*, 2007, **318**, 426–430.
37 G.-A. Junter, P. Thébault and L. Lebrun, *Acta Biomater.*, 2016, **30**, 13–25.
38 E. Joseph, A. Patil, S. Hirlekar, A. Shete, N. Parekh, A. Prabhune and A. Nisal, *ACS Appl. Bio Mater.*, 2019, **2**, 675–684.
39 S. Geißler, M. Gomez-Florit, D. Wiedmer, A. Barrantes, F. C. Petersen and H. Tiainen, *ACS Biomater. Sci. Eng.*, 2019, **5**, 3340–3351.
40 L. Q. Xu, K.-G. Neoh and E.-T. Kang, *Prog. Polym. Sci.*, 2018, **87**, 165–196.
41 J. Zhou, Z. Lin, Y. Ju, M. A. Rahim, J. J. Richardson and F. Caruso, *Acc. Chem. Res.*, 2020, **53**, 1269–1278.
42 T. S. Sileika, D. G. Barrett, R. Zhang, K. H. A. Lau and P. B. Messersmith, *Angew. Chem.*, 2013, **125**, 10966–10970.
43 Z. Guo, W. Xie, J. Lu, X. Guo, J. Xu, W. Xu, Y. Chi, N. Takuya, H. Wu and L. Zhao, *J. Mater. Chem. B*, 2021, **9**, 4098–4110.
44 L. Q. Xu, D. Pranantyo, K.-G. Neoh, E.-T. Kang and G. D. Fu, *ACS Sustainable Chem. Eng.*, 2016, **4**, 4264–4272.
45 G. Dong, H. Liu, X. Yu, X. Zhang, H. Lu, T. Zhou and J. Cao, *Nat. Prod. Res.*, 2018, **32**, 2225–2228.
46 M. Nakayama, K. Suzuki, M. Toda, S. Okubo, Y. Hara and T. Shimamura, *Antiviral Res.*, 1993, **21**, 289–299.
47 Y. Du, W. Z. Qiu, Z. L. Wu, P. F. Ren, Q. Zheng and Z. K. Xu, *Adv. Mater. Interfaces*, 2016, **3**, 1600167.
48 P. Wang, J. Liu, X. Luo, P. Xiong, S. Gao, J. Yan, Y. Li, Y. Cheng and T. Xi, *J. Mater. Chem. B*, 2019, **7**, 7314–7325.
49 H. Ejima, J. J. Richardson, K. Liang, J. P. Best, M. P. van Koeverden, G. K. Such, J. Cui and F. Caruso, *Science*, 2013, **341**, 154–157.
50 Y. Cao, R. Zheng, X. Ji, H. Liu, R. Xie and W. Yang, *Langmuir*, 2014, **30**, 3876–3882.
51 L. Liu, C. Ge, Y. Zhang, W. Ma, X. Su, L. Chen, S. Li, L. Wang, X. Mu and Y. Xu, *Biomater. Sci.*, 2020, **8**, 4852–4860.
52 C. Zhang, D.-F. Hu, J.-W. Xu, M.-Q. Ma, H. Xing, K. Yao, J. Ji and Z.-K. Xu, *ACS Nano*, 2018, **12**, 12347–12356.
53 L. Liu, H. Shi, H. Yu, R. Zhou, J. Yin and S. Luan, *Biomater. Sci.*, 2019, **7**, 5035–5043.
54 H. Cai, P. Wang and D. Zhang, *J. Drug Delivery Sci. Technol.*, 2019, **54**, 101251.
55 S. Ulusan, V. Bütün, S. Banerjee and I. Erel-Goktepe, *Langmuir*, 2018, **35**, 1156–1171.
56 E. Cagli, E. Ugur, S. Ulusan, S. Banerjee and I. Erel-Goktepe, *Eur. Polym. J.*, 2019, **114**, 452–463.
57 H. Liu, Z. Liu, X. Liu, H. Zhong, L. Mo, C. Chen, Z. Guo and B. Ye, *Colloid Interface Sci. Commun.*, 2021, **41**, 100383.
58 Y. Wang, Y. Zou, Y. Wu, T. Wei, K. Lu, L. Li, Y. Lin, Y. Wu, C. Huang and Y. Zhang, *ACS Appl. Mater. Interfaces*, 2021, **13**, 48403–48413.
59 T.-W. Chang, H. Ko, W.-S. Huang, Y.-C. Chiu, L.-X. Yang, Z.-C. Chia, Y.-C. Chin, Y.-J. Chen, Y.-T. Tsai and C.-W. Hsu, *Chem. Eng. J.*, 2022, **428**, 131237.
60 D. Pranantyo, L. Q. Xu, E.-T. Kang and M. B. Chan-Park, *Biomacromolecules*, 2018, **19**, 2156–2165.
61 B. Onat, S. Ozcubukcu, S. Banerjee and I. Erel-Goktepe, *Eur. Polym. J.*, 2018, **103**, 101–115.
62 Y. Li, X. Wang and J. Sun, *Chem. Soc. Rev.*, 2012, **41**, 5998–6009.
63 J. Fu, J. Ji, W. Yuan and J. Shen, *Biomaterials*, 2005, **26**, 6684–6692.
64 A. L. Becker, A. P. Johnston and F. Caruso, *Small*, 2010, 6.
65 M. Keeney, X. Jiang, M. Yamane, M. Lee, S. Goodman and F. Yang, *J. Mater. Chem. B*, 2015, **3**, 8757–8770.
66 X. Zhu and X. J. Loh, *Biomater. Sci.*, 2015, **3**, 1505–1518.
67 T. Wei, W. Zhan, L. Cao, C. Hu, Y. Qu, Q. Yu and H. Chen, *ACS Appl. Mater. Interfaces*, 2016, **8**, 30048–30057.
68 M. Criado-Gonzalez, C. Mijangos and R. Hernández, *Polymers*, 2021, **13**, 2254.
69 P.-F. Ren, H.-C. Yang, H.-Q. Liang, X.-L. Xu, L.-S. Wan and Z.-K. Xu, *Langmuir*, 2015, **31**, 5851–5858.
70 H. Xu, W.-p. Huang, K.-f. Ren and Y.-m. Tang, *Colloid Interface Sci. Commun.*, 2021, **42**, 100422.
71 M. Campinas, R. M. Viegas and M. J. Rosa, *Water Res.*, 2013, **47**, 5690–5699.
72 M. A. Rahim, H. Ejima, K. L. Cho, K. Kempe, M. Müllner, J. P. Best and F. Caruso, *Chem. Mater.*, 2014, **26**, 1645–1653.
73 L. Peng, F. Cheng, Y. Zheng, Z. Shi and W. He, *Langmuir*, 2018, **34**, 10748–10756.
74 I. Erel-Unal and S. A. Sukhishvili, *Macromolecules*, 2008, **41**, 3962–3970.
75 I. Zhuk, F. Jariwala, A. B. Attygalle, Y. Wu, M. R. Libera and S. A. Sukhishvili, *ACS Nano*, 2014, **8**, 7733–7745.
76 F. Hizal, I. Zhuk, S. Sukhishvili, H. J. Busscher, H. C. van der Mei and C.-H. Choi, *ACS Appl. Mater. Interfaces*, 2015, **7**, 20304–20313.
77 G. Xu, D. Pranantyo, B. Zhang, L. Xu, K.-G. Neoh and E.-T. Kang, *RSC Adv.*, 2016, **6**, 14809–14818.
78 M. H. Iqbal, A. Schroder, H. Kerdjoudj, C. Njel, B. Senger, V. Ball, F. Meyer and F. Boulmedais, *ACS Appl. Mater. Interfaces*, 2020, **12**, 22601–22612.
79 R. Fernandes, L.-Q. Wu, T. Chen, H. Yi, G. W. Rubloff, R. Ghodssi, W. E. Bentley and G. F. Payne, *Langmuir*, 2003, **19**, 4058–4062.
80 M. Saita, T. Ikeda, M. Yamada, K. Kimoto, M. C.-I. Lee and T. Ogawa, *Int. J. Nanomed.*, 2016, **11**, 223.
81 T. Lee, H. Abdullah, P. Koshy and M. Idris, *Thin Solid Films*, 2018, **660**, 191–198.
82 D. Luo, T. Zhang and I. Zhitomirsky, *J. Colloid Interface Sci.*, 2016, **469**, 177–183.
83 J. Sun, Y. Zhu, L. Meng, P. Chen, T. Shi, X. Liu and Y. Zheng, *Acta Biomater.*, 2016, **45**, 387–398.
84 L. Meng, K. Pan, Y. Zhu, W. Wei, X. Li and X. Liu, *ACS Biomater. Sci. Eng.*, 2018, **4**, 4122–4131.
85 X. He, K. Gopinath, G. Sathishkumar, L. Guo, K. Zhang, Z. Lu, C. Li, E.-T. Kang and L. Xu, *ACS Appl. Mater. Interfaces*, 2021, **13**, 20708–20717.

86 N. Esfandiari, A. Simchi and R. Bagheri, *J. Biomed. Mater. Res. Part A*, 2014, **102**, 2625–2635.
87 X. Tang, X. Zhang, Y. Chen, W. Zhang, J. Qian, H. Soliman, A. Qu, Q. Liu, S. Pu, N. Huang and G. Wan, *Mater. Sci. Eng., C*, 2020, **108**, 110487.
88 F. Behboodi-Sadabad, H. Zhang, V. Trouillet, A. Welle, N. Plumere and P. A. Levkin, *Chem. Mater.*, 2018, **30**, 1937–1946.
89 N. Hadjesfandiari, K. Yu, Y. Mei and J. N. Kizhakkedathu, *J. Mater. Chem. B*, 2014, **2**, 4968–4978.
90 D. Mitra, E.-T. Kang and K. G. Neoh, *ACS Appl. Polym. Mater.*, 2021, **3**, 2233–2263.
91 G. Gao, D. Lange, K. Hilpert, J. Kindrachuk, Y. Zou, J. T. Cheng, M. Kazemzadeh-Narbat, K. Yu, R. Wang and S. K. Straus, *Biomaterials*, 2011, **32**, 3899–3909.
92 L. Liu, W. Peng, X. Zhang, J. Peng, P. Liu and J. Shen, *J. Mater. Sci. Technol.*, 2021, **62**, 96–106.
93 U. Ajdnik, L. F. Zemljič, O. Plohl, L. Pérez, J. Trček, M. Bračič and T. Mohan, *ACS Appl. Mater. Interfaces*, 2021.
94 V. Yesilyurt, O. Veiseh, J. C. Doloff, J. Li, S. Bose, X. Xie, A. R. Bader, M. Chen, M. J. Webber and A. J. Vegas, *Adv. Healthcare Mater.*, 2017, **6**, 1601091.
95 Z. Wang, H.-C. Yang, F. He, S. Peng, Y. Li, L. Shao and S. B. Darling, *Matter*, 2019, **1**, 115–155.
96 D. Pranantyo, L. Q. Xu, K.-G. Neoh, E.-T. Kang, Y. X. Ng and S. L.-M. Teo, *Biomacromolecules*, 2015, **16**, 723–732.
97 L. Xu, D. Pranantyo, K.-G. Neoh and E.-T. Kang, *ACS Sustainable Chem. Eng.*, 2017, **5**, 3055–3062.
98 G. Xu, P. Liu, D. Pranantyo, K.-G. Neoh, E.-T. Kang and S. Lay-Ming Teo, *ACS Sustainable Chem. Eng.*, 2019, **7**, 1786–1795.
99 G. Xu, K. G. Neoh, E.-T. Kang and S. L.-M. Teo, *ACS Sustainable Chem. Eng.*, 2020, **8**, 2586–2595.
100 L. L. Guo, Y. F. Cheng, X. Ren, K. Gopinath, Z. S. Lu, C. M. Li and L. Q. Xu, *Colloids Surf., B*, 2021, **200**, 111592.
101 J. Ren, R. Kong, Y. Gao, L. Zhang and J. Zhu, *J. Colloid Interface Sci.*, 2021, **602**, 406–414.
102 S. Chen, Y. Xie, T. Xiao, W. Zhao, J. Li and C. Zhao, *Chem. Eng. J.*, 2018, **337**, 122–132.
103 Y. Qiao, Q. Zhang, Q. Wang, Y. Li and L. Wang, *Acta Biomater.*, 2021, **128**, 277–290.
104 H. Tan, J. Sun, D. Jin, J. Song, M. Lei, A. Antoshin, X. Chen, M. Yin, X. Qu and C. Liu, *Biomater. Sci.*, 2020, **8**, 3334–3347.
105 Q. Zhang, Y. Qiao, C. Li, J. Lin, H. Han, X. Li, J. Mao, F. Wang and L. Wang, *Carbohydr. Polym.*, 2021, 118246.
106 Q. Zhang, Y. Qiao, J. Zhu, Y. Li, C. Li, J. Lin, X. Li, H. Han, J. Mao and F. Wang, *Composites, Part B*, 2021, **223**, 109140.
107 Z. Hanif, Z. A. Khan, M. F. Siddiqui, M. Z. Tariq, S. Park and S. J. Park, *Carbohydr. Polym.*, 2020, **231**, 115746.
108 X. Wang, W. Cai, D. Ye, Y. Zhu, M. Cui, J. Xi, J. Liu and W. Xing, *Composites, Part B*, 2021, **224**, 109206.
109 H. Peng, D. Wang and S. Fu, *Chem. Eng. J.*, 2020, **384**, 123288.
110 H. Wu, H. Sun, W. Hong, L. Mao and Y. Liu, *ACS Appl. Mater. Interfaces*, 2017, **9**, 32255–32263.
111 U. Boro and N. Karak, *Prog. Org. Coat.*, 2017, **104**, 180–187.
112 S. A. Aromal and D. Philip, *Phys. E*, 2012, **44**, 1692–1696.
113 X. He, G. Sathishkumar, K. Gopinath, K. Zhang, Z. Lu, C. Li, E.-T. Kang and L. Xu, *Chem. Eng. J.*, 2021, **421**, 130005.
114 H. Tang, Y. Zhao, X. Yang, D. Liu, P. Shao, Z. Zhu, S. Shan, F. Cui and B. Xing, *Environ. Sci. Technol.*, 2017, **51**, 9674–9682.
115 A. Ali, M. Sattar, F. Hussain, M. H. K. Tareen, J. Militky and M. T. Noman, *Nanomaterials*, 2021, **11**, 1007.
116 H. Di, L. Qiaoxia, Z. Yujie, L. Jingxuan, W. Yan, H. Yinchun, L. Xiaojie, C. Song and C. Weiyi, *Surf. Coat. Technol.*, 2020, **399**, 126169.
117 J. H. Park, S. Choi, H. C. Moon, H. Seo, J. Y. Kim, S.-P. Hong, B. S. Lee, E. Kang, J. Lee and D. H. Ryu, *Sci. Rep.*, 2017, **7**, 1–7.
118 J. Yao, Y. Sun, M. Yang and Y. Duan, *J. Mater. Chem.*, 2012, **22**, 14313–14329.
119 S. Gnanasekar, P. Palanisamy, P. K. Jha, J. Murugaraj, M. Kandasamy, A. M. K. Mohamed Hussain and S. Sivaperumal, *ACS Sustainable Chem. Eng.*, 2018, **6**, 349–363.
120 S. Gnanasekar, D. Balakrishnan, P. Seetharaman, P. Arivalagan, R. Chandrasekaran and S. Sivaperumal, *ACS Appl. Nano Mater.*, 2020, **3**, 4574–4585.
121 X. Xie, C. Mao, X. Liu, Y. Zhang, Z. Cui, X. Yang, K. W. Yeung, H. Pan, P. K. Chu and S. Wu, *ACS Appl. Mater. Interfaces*, 2017, **9**, 26417–26428.
122 L. Q. Xu, Y. B. Liao, N. N. Li, Y. J. Li, J. Y. Zhang, Y. B. Wang, X. F. Hu and C. M. Li, *J. Colloid Interface Sci.*, 2018, **514**, 733–739.
123 H. Li, C. Gao, L. Tang, C. Wang, Q. Chen, Q. Zheng, S. Yang, S. Sheng and X. Zan, *ACS Appl. Bio Mater.*, 2019, **3**, 673–684.
124 Y. Zhang, L. Shen, Q.-Z. Zhong and J. Li, *Colloids Surf., B*, 2021, 111851.
125 Q. Li, W. Xiao, F. Zhang, Q. Liu, J. Ye, H. Dong and X. Cao, *J. Mater. Chem. B*, 2018, **6**, 2734–2738.
126 Z. Xu, X. Wang, X. Liu, Z. Cui, X. Yang, K. W. K. Yeung, J. C. Chung, P. K. Chu and S. Wu, *ACS Appl. Mater. Interfaces*, 2017, **9**, 39657–39671.
127 Y. Liu, S. Mao, L. Zhu, S. Chen and C. Wu, *Eur. Polym. J.*, 2021, **153**, 110498.
128 Y. Qiao, Q. Zhang, Q. Wang, J. Lin, J. Wang, Y. Li and L. Wang, *ACS Appl. Mater. Interfaces*, 2021, **13**, 35456–35468.
129 M. He, X. Gao, Y. Fan, L. Xie, M. Yang and W. Tian, *J. Mater. Chem. B*, 2021, **9**, 1096–1106.
130 X. Yang, P. Huang, H. Wang, S. Cai, Y. Liao, Z. Mo, X. Xu, C. Ding, C. Zhao and J. Li, *Colloids Surf., B*, 2017, **160**, 136–143.
131 E. Yılmaz, B. Çakıroğlu, A. Gökçe, F. Findik, H. O. Gulsoy, N. Gulsoy, Ö. Mutlu and M. Özacar, *Mater. Sci. Eng., C*, 2019, **101**, 292–305.
132 S. Yang, Y. Wang, X. Wu, S. Sheng, T. Wang and X. Zan, *ACS Biomater. Sci. Eng.*, 2019, **5**, 3582–3594.

133 Y. Wang, S. Liu, K. Ding, Y. Zhang, X. Ding and J. Mi, *J. Mater. Chem. B*, 2021, **9**, 4746–4762.
134 Y. F. Cheng, D. Pranantyo, G. Kasi, Z. S. Lu, C. M. Li and L. Q. Xu, *Biomater. Sci.*, 2020, **8**, 2120–2128.
135 F. Reitzer, M. Allais, V. Ball and F. Meyer, *Adv. Colloid Interface Sci.*, 2018, **257**, 31–41.
136 J. Huang, Y. Cheng, Y. Wu, X. Shi, Y. Du and H. Deng, *Int. J. Biol. Macromol.*, 2019, **139**, 191–198.
137 T. Wei, Q. Yu and H. Chen, *Adv. Healthcare Mater.*, 2019, **8**, 1801381.
138 M. Kumorek, I. M. Minisy, T. Krunclová, M. Voršiláková, K. Venclíková, E. M. Chánová, O. Janoušková and D. Kubies, *Mater. Sci. Eng., C*, 2020, **109**, 110493.
139 L. Sutrisno, S. Wang, M. Li, Z. Luo, C. Wang, T. Shen, P. Chen, L. Yang, Y. Hu and K. Cai, *J. Mater. Chem. B*, 2018, **6**, 5290–5302.
140 A. V. Singhal, D. Malwal, S. Thiyagarajan and I. Lahiri, *Prog. Org. Coat.*, 2021, **159**, 106421.
141 A. Rodríguez-Contreras, D. Torres, B. Rafik, M. Ortiz-Hernandez, M. P. Ginebra, J. A. Calero, J. M. Manero and E. Ruperez, *Surf. Coat. Technol.*, 2021, **421**, 127476.
142 P. Li, W. She, Y. Luo, D. He, J. Chen, N. Ning, Y. Yu, S. De Beer and S. Zhang, *J. Mater. Chem. B*, 2021, **9**, 159–169.
143 J. Zeng, Y. Wang, Z. Sun, H. Chang, M. Cao, J. Zhao, K. Lin and Y. Xie, *Chem. Eng. J.*, 2020, **394**, 125017.
144 X. Ren, R. Gao, H. C. Van der Mei, Y. Ren, B. W. Peterson and H. J. Busscher, *ACS Appl. Mater. Interfaces*, 2020, **12**, 34610–34619.
145 Y. Chen, Y. Gao, Y. Chen, L. Liu, A. Mo and Q. Peng, *J. Controlled Release*, 2020, **328**, 251–262.
146 S. Cabana, C. S. Lecona-Vargas, H. I. Meléndez-Ortiz, A. Contreras-García, S. Barbosa, P. Taboada, B. Magarinos, E. Bucio, A. Concheiro and C. Alvarez-Lorenzo, *J. Drug Delivery Sci. Technol.*, 2017, **42**, 245–254.
147 H. Li, S. Yan, L. Wu and S. Dou, *World J. Eng. Technol.*, 2021, **9**, 60.
148 Z. Yu, L. Jiang, R. Liu, W. Zhao, Z. Yang, J. Zhang and S. Jin, *Chem. Eng. J.*, 2021, **426**, 131914.
149 Y.-Q. Zhao, Y. Sun, Y. Zhang, X. Ding, N. Zhao, B. Yu, H. Zhao, S. Duan and F.-J. Xu, *ACS Nano*, 2020, **14**, 2265–2275.
150 Y. Wang, T. Wei, Y. Qu, Y. Zhou, Y. Zheng, C. Huang, Y. Zhang, Q. Yu and H. Chen, *ACS Appl. Mater. Interfaces*, 2020, **12**, 21283–21291.
151 L. Huang, G. Szewczyk, T. Sarna and M. R. Hamblin, *ACS Infect. Dis.*, 2017, **3**, 320–328.
152 M. Abbas, Q. Zou, S. Li and X. Yan, *Adv. Mater.*, 2017, **29**, 1605021.
153 M. Qi, M. Chi, X. Sun, X. Xie, M. D. Weir, T. W. Oates, Y. Zhou, L. Wang, Y. Bai and H. H. Xu, *Int. J. Nanomed.*, 2019, **14**, 6937.
154 Z. K. Zander and M. L. Becker, *ACS Macro Lett.*, 2018, **7**, 16–25.
155 Y. F. Cheng, Y. H. Mei, G. Sathishkumar, Z. S. Lu, C. M. Li, F. Wang, Q. Y. Xia and L. Q. Xu, *Colloid Interface Sci. Commun.*, 2020, **35**, 100241.
156 B. L. Tardy, J. J. Richardson, V. Nithipipat, K. Kempe, J. Guo, K. L. Cho, M. A. Rahim, H. Ejima and F. Caruso, *Biomacromolecules*, 2019, **20**, 1421–1428.
157 L. Yang, L. Han, Q. Liu, Y. Xu and L. Jia, *Acta Biomater.*, 2017, **64**, 187–199.